R E V I E W

IONPs-Based Medical Imaging in Cancer Care: Moving Beyond Traditional Diagnosis and Therapeutic Assessment

Xiaolin Yan, Shanshan Li, Haiyin Yan, Chungang Yu, Fengxi Liu

Department of Clinical Pharmacy, The First Affiliated Hospital of Shandong First Medical University & Shandong Provincial Qianfoshan Hospital, Shandong Engineering and Technology Research Center for Pediatric Drug Development, Shandong Medicine and Health Key Laboratory of Clinical Pharmacy, Jinan, Shandong Province, People's Republic of China

Correspondence: Fengxi Liu, Tel +86 0531-89269594, Email sdliufengxi@163.com

Abstract: Cancer-related burden of morbidity and mortality is rapidly rising worldwide. Medical imaging plays an important role in every phase of cancer management, including diagnosis, staging, treatment planning and evaluation. Iron oxide nanoparticles (IONPs) could serve as contrast agents or labeling agents to enhance the identification and visualization of pathological tissues as well as target cells. Multimodal or multifunctional imaging can be easily acquired by modifying IONPs with other imaging agents or functional groups, allowing the accessibility of combined imaging techniques and providing more comprehensive information for cancer care. To date, IONPs-enhanced medical imaging has gained intensive application in early diagnosis, monitoring treatment as well as guiding radio-frequency ablation, sentinel lymph node dissection, radiotherapy and hyperthermia therapy. Besides, IONPs mediated imaging is also capable of promoting the development of anti-cancer nanomedicines through identifying patients potentially sensitive to nanotherapeutics. Based on versatile imaging modes and application fields, this review highlights and summarizes recent research advances of IONPs-based medical imaging in cancer management. Besides, currently existing challenges are also discussed to provide perspectives and advices for the future development of IONPs-based imaging in cancer management.

Keywords: iron oxide nanoparticles, medical imaging, early diagnosis, treatment evaluation, personalized treatment

Introduction

Cancer is the leading cause of death worldwide, with both incidence and mortality increasing rapidly.[1] Notably, 19.3 million new cases and almost 10.0 million deaths were estimated by the International Agency for Research on Cancer (IARC) worldwide in 2020. It is anticipated that the cancer burden would be 28.4 million cases by 2040, a 47% rise from 2020.[1,2] In order to improve the quality of life and prolong the progression-free survival period (PFS) of cancer patients, early diagnosis and precise treatment are necessary. Therefore, the clinical demands for novel and sensitive approaches to optimize the diagnosis and therapeutics of cancer are always there.

As is known, medical imaging plays a key role in cancer diagnosis and treatment evaluation.[3–5] Due to their uniquely favorable biocompatibility and pharmacokinetics, as well as outstanding competency in promoting diagnosis and therapy, IONPs have received intensive exploration in medical imaging. Specifically, IONPs for medical imaging are crystals of Fe_3O_4 or γ-Fe_2O_3 with particle diameter in the range of 1–1000 nm. Upon covering the hydrophilic shell, the modified IONPs can gain improved stability in blood circulation and the potential for biomedical imaging. Over the past few decades, a variety of commercial products have been on the market, such as Ferumoxide, Ferucarbotran, Ferumoxytol, Ferumoxtran, etc. (showed in Table 1),[6–15] making IONPs readily available for direct clinic or "off-label" use in medical imaging and more favorable than other candidates undergoing experimental analysis.

In recent years, IONPs-based imaging has displayed uniquely superior performance in cancer management. In this review, fundamental knowledges, covering the theories, advantages, and challenges of the imaging modes of IONPs-based imaging are outlined. Next, an overview of IONPs-based imaging in cancer diagnosis and therapeutic optimization,

Table 1 General Information of Commercial and Tailored IONPs Suitable for Cancer Imaging

Generic Name	Trade Name	Hydrodynamic Diameter (nm)	Coating Materials	Imaging Method	Applications
Ferumoxide	Feridex	50–100	Dextran	T2-weighted MRI	Liver cancer imaging[6]
Ferucarbotran	Resovist	80	Carboxy-dextran	T2-weighted MRI	Liver cancer imaging[7] Lymph node imaging[8]
Ferumoxytol	Feraheme	17–31	Carboxymethyl-dextran	T2-weighted MRI	Angiography[9] Lymph node imaging[10]
Ferumoxtran-10	Combidex	15–30	Dextran	T2-weighted MRI	Angiography[11] Lymph node imaging[12]
Feruglose	Clariscan	20	PEGylated starch	T2-weighted MRI	Angiography[13]
Tailored IONPs	n.a.	40	PEG	MPI	Guiding Hyperthermia Therapy[22]
Tailored IONPs	n.a.	20	Zwitterionic structure containing polyacrylic acid and diethylamino	T2 imaging	Angiography[87]
Tailored IONPs	n.a.	100	Dextran	T2 imaging	CTC detection[99]
Tailored IONPs	n.a.	32	Dextran	T2 imaging	Tracking Therapeutic Cells[127]
Tailored IONPs	n.a.	32	PEG	T2 imaging	Promotion of nanomedicine development[119]

including basic principle, research condition, future prospect and clinical translation barrier, are discussed in detail. Related studies are selected to elaborate these prevalent applications and provide references for research with similar areas of interest.

Primary Modes of IONPs-Based Medical Imaging in Cancer Care
MRI

Owing to free of radiation, strong soft tissue contrast, no depth limit, and multi-directional and multi-sequence imaging, MRI is exquisitely suitable for tumor imaging, especially for highly heterogeneous tumors, where a specimen alone cannot represent whole tumor mass. Contrast agents can be used to enhance the contrast between tumors and normal tissues, thus improving the sensitivity of MRI. In clinic, MRI contrast agents can be divided into two major types: (1) positive T1-weighted contrast agents represented by Gd-chelates, which mainly accelerate T1 relaxation and generate an overall bright image through dipole–dipole interactions with local water protons. (2) negative T2 contrast agents represented by IONPs, which effectively shorten the T2 time and produce dark image. In principle, when exposed to an external magnetic field, IONPs could be induced to generate a stronger local magnetic field and thus affect the relaxation process of surrounding water molecules, finally generating enhanced MRI image.[16]

IONPs possess many attractive properties compared with other contrast agents, such as Gd-chelates and radionuclides. Firstly, IONPs enjoy good biocompatibility and safety. (1) In terms of metabolism and elimination, IONPs can be biodegraded into ferric ions in lysosome or endosome and then participate in physiological iron homeostasis;[17] (2) owing to larger apparent molecular weight and larger size, IONPs can also avoid unpredictable long-term toxicity in brain or kidney and are especially safe for patients with kidney and brain disorders. In contrast, Gd-based contrast agents are linked to neurotoxicity or nephrotoxicity resulting from their free penetration through all the physical barriers; (3) unlike radionuclides, IONPs are highly maneuverable and safe in observation and no worry of radio harm, respectively. (4) IONPs-enhanced contrast effect is also more sensitive than that of Gd-chelates. Superparamagnetic IONPs have higher relaxation efficiency than paramagnetic Gd-based contrast agents, resulting in greater detection sensitivity. By

calculating in terms of the concentration of fundamental contrast units (eg, gadolinium and iron ions), the detection limit is 10^{-7} mol/L of IONPs against 10^{-6} mol/L for Ga-DTPA according to the published reports.[18]

Although IONPs-enhanced MRI is relatively mature and reliable, there are still several problems constraining further application. Firstly, the intrinsic dark T2 images might be confused with some non-tumor physiopathological conditions, such as hemorrhage, calcification, necrosis, metal deposits, air–tissue boundaries and other hypointense areas.[19,20] Furthermore, the large magnetic moments of T2 contrast agents could destroy the background around disease regions, generating unclear images. To overcome this weakness mentioned above, ultra-small IONPs with core diameter <5nm have been proven to act as promising T1 contrast agents.[19] Secondly, synthesis conditions that could precisely control the interrelated parameters (size, morphology, surface chemistry, etc.) to maintain the stability and bioavailability of IONPs in vivo are always harsh, especially for ultra-small IONPs. Thirdly, there are still some concerns for the potential unknown toxicity of IONPs, such as damage to DNA and mitochondrion, interfering with signal transduction and iron homeostasis, as well as risks of eliciting anaphylactoid reactions.[19,20] By successfully overcoming these bottlenecks, IONPs-enhanced MRI would make significant strides to clinical application.

MPI

As a novel imaging technique, MPI could produce highly sensitive and specific images by directly measuring the location and concentration of IONPs in vivo, depending on strong static gradient magnetic field (selected field) and time-varying, weak field (excitation field) for spatial localization and excitation.[21,22] Under the selected field, IONPs outside the field-free region (FFR), where magnetic field is zero, are magnetically saturated and have no magnetization response. Only the IONPs in FFR can align with excitation field, thus generating magnetization changes and releasing MPI signals. As the gradient magnetic field and FFR continuously scan over the region of interest, the quantity and spatial distribution of IONPs at every site of the body will be collected.[23]

As a tracer imaging technique with utilization of IONPs as tracing agents, MPI enjoys some merits over conventional MRI. Firstly, MPI is linearly quantitative with the signal intensity directly proportional to the number of IONPs near FFR, and the wide linear range covers four orders of magnitude.[24] Secondly, MPI is highly sensitive with signal intensity of MPI tracing agent (Ferucarbotran, also known as Vivotrax) 2.3 times as high as MRI contrast agent (Ferumoxytol) at the same concentration of Fe. MPI signal of tailored IONPs that are modified with copolymer poly(styrene-co-maleic anhydride) is proven to be 7 times as high as the MRI signal of ferumoxytol. As previously reported, MPI is capable of noninvasively cell tracking with as little as 250-cells (with an average uptake of Fe at 0.555 pmol/cell), while 2500 labeled cells were hardly distinguishable in tailored IONPs-enhanced MRI.[25] Thirdly, MPI has sub-mm resolution, which is not inferior to MRI. With improved tracing agents, the resolution of MPI can further be increased to about 600 μm.[26] Fourthly, since low frequency magnetic field is used in MPI and only IONPs are visualized, there is no background interference from the surrounding tissues and worries about depth attenuation.[20] Therefore, MPI is especially suitable to detect certain tissues where the endogenous MRI signal is too low to provide enough contrast, such as blood vessels, dense connective tissues and air–tissue boundaries (lung, gastrointestinal tract).[20]

Since IONPs are the only source of MPI signal, both the iron oxide core and surface modification should be optimized to obtain preferable resolution and pharmacokinetics. Usually, IONPs for MPI are with a core diameter of 15–35 nm, and a hydrodynamic radius of about 100 nm after modification.[25–27] A few tailored IONPs with uniform size have been developed, which achieved clear MPI images with high signal-to-noise ratios in xenograft animal models.[25–27] However, until now, MPI is only commercially available for small animals and has not yet been accepted for clinical application, partially due to the lack of available scanning systems for human. Additionally, MPI alone could not provide anatomical information. Thus, combination with CT or MRI is required to identify the location of lesion sites. In the future, more efforts should be made to solve the limitations and promote clinical translation of MPI.

Fluorescent Imaging

Conventional MRI lacks the sensitivity to achieve cellular-level detection. Fluorescent imaging (FI) enables noninvasive visualization and characterization of cancer-related changes at the cellular and even molecular level, which could facilitate the quantitative analysis of pathophysiological functions.[28–30] After decorating the facile surface with

fluorophores (eg, methylene blue, fluorescein sodium or indocyanine green) and tumor-specific ligands (eg, antibodies or targeting peptides), IONPs could combine target tumor cells with high affinity. As a result, tumor cells are labeled with fluorophores and allow optical visualization. With the remarkable advantages of high brightness, simple procedure and good cost-effectiveness, FI has been widely used in pathological analysis of biopsies as well as characterization of targeted cells and molecules. Furthermore, different cells or molecules could be marked and observed simultaneously with multicolor FI.[31] Since the quench of fluorescence signals by native tissues in the near-infrared (NIR, 650–900 nm) region is minimal, IONPs conjugated with NIR emitting fluorescent dye (eg, indocyanine green) can achieve penetration depth of several millimeters.[32,33]

Nowadays, FI has been clinically used to measure target tumor cells and molecules in vitro. Lots of researches have highlighted the great potential of IONPs-based fluorescence hybrids for successful diagnosis and delineation of various solid tumors in animal models.[33,34] However, FI still has poor penetration depth because of weak signal for deep tissues. In addition, FI provides poor specificity due to the interference of auto-fluorescence of native tissues. One potential in vivo application of IONPs-based fluorescence probes is margin delineation of surface tumors, such as breast cancer, gastrointestinal cancer and oropharyngeal cancer via MRI-fluorescence dual-modal imaging.[31]

Dual-Modal Imaging

In some situations, single-mode imaging is not adequate to provide comprehensive information for accurate diagnosis. Multimodal imaging referring to simultaneous integration of dual or multiple imaging modes into a single imaging technique is now increasingly preferred to improve early detection and localization of cancer.[35] Multimodal imaging can provide both anatomical information (through CT, MRI) and molecular or functional information (through PET, SPECT, MPI) to fully elaborate tumor characteristics, including localization, progression, contour, viability, etc.[36] Recently, clinical availability of scanners for integrated positron emission tomography/CT (PET/CT), PET/MRI and single-photon emission computed tomography/MRI (PECT/MRI) has enabled the practical potential of multimodal imaging to be explored.

Typically, multimodal imaging agents are needed to collect imaging signal of each imaging mode and obtain comprehensive information for multi-modal imaging techniques. Due to intrinsic good biocompatibility and easy surface modification, IONPs are favorable options for constructing multimodal agents. The application of IONPs-based multi-modal agents can bring some improvements in detection accuracy. In terms of PET/MRI, a clinically available multi-modal imaging technique, the modified IONPs can increase the lifetime and targeting efficacy of radiotracers, thus providing more observation time. In addition, the use of IONPs allows drug delivery, hyperthermia or photodynamic therapy, which endows PET/MRI with theragnostic activity.[37] However, common concerns of IONPs-based imaging also hinder their clinical translation. Further works should be devoted to improve IONPs (better pharmacokinetics and targeting ability) and imaging instruments (better resolution, miniaturization, lower cost, more intelligence, etc.) to accelerate the development of multimodal imaging technique.

Application of IONPs in Guiding Tumor Therapy and Evaluating Therapeutic Effect

Image-Guided Therapy

Cancer Care

Liver cancer is one of the most common malignant tumors and ranks as the third leading cause of cancer-related death worldwide.[1] Early diagnosis and precise positioning of the lesion are necessary to prolong the survival time. IONPs with hydrodynamic diameter of 50–150 nm could be employed as specific MRI contrast agents to discern malignant hepatocellular carcinoma (HCC) from normal liver tissue. Kupffer cells are phagocytic macrophages resident in healthy liver parenchyma, which can specifically take up and store IONPs in the form of clusters in the lysosome. Nevertheless, Kupffer cells are found to be absent or scarce in hepatic lesions, leading to lower macrophage uptake of IONPs. Accordingly, less signal intensity (SI) loss and relative brighter image in MRI would appear for malignant liver lesion against the dark background of healthy liver or benign focal hepatic lesions following IONPs administration.[14,38]

Moreover, SI loss is considered to be related to the histological grade of tumor.[39] For example, the mean percentage of SI loss was higher in solid benign lesions than in malignant lesions (39.6% vs 3.2%, P < 0.05).[38] Consequently, several IONPs, such as Ferumoxide and Ferucarbotran have been already applied to discern malignant focal liver lesions from non-tumor parenchyma in clinic, thus guiding localization of the surgical treatment and interventional procedures.[38]

It is worth noting that false-negative results may occur for IONPs-enhanced MRI when small and well-differentiated HCCs exist. The underlying mechanism is that a considerable number of Kupffer cells have been found in well-differentiated HCCs.[6,39] Fortunately, several studies have demonstrated the availability of T2*-weighted MRI for differentiating well-differentiated HCCs (WD-HCCs) from dysplastic nodules (DNs) and moderately/poorly differentiated HCCs (MD/PD-HCCs).[7,38] Along with high magnetic field, T2*-weighted imaging could enlarge the subtle difference among various liver lesions and make them significant.[7,40] In the study carried out by Park et al, the enhancement patterns of SI were divided into six categories: (1) heterogeneous strong high SI; (2) homogenous strong high SI; (3) incomplete high SI; (4) iso SI; and (5) low SI. In Ferucarbotran-enhanced T2 image, DNs mainly showed low- or iso SI. However, 40.5% WD-HCC also exhibited iso SI, thus easily misdiagnosed as DNs (Figure 1A). On T2* image, WD-HCCs were inclined to show incomplete high SI, while DNs showed low- or iso SI and the majority of MD-/PD- HCCs showed homogeneous or heterogeneous strong high SI, respectively (Figure 1B).[7] For example, the WD-HCC confirmed by pathologic examination was misdiagnosed as DNs in T2-weighted imaging (Figure 1C and D), while
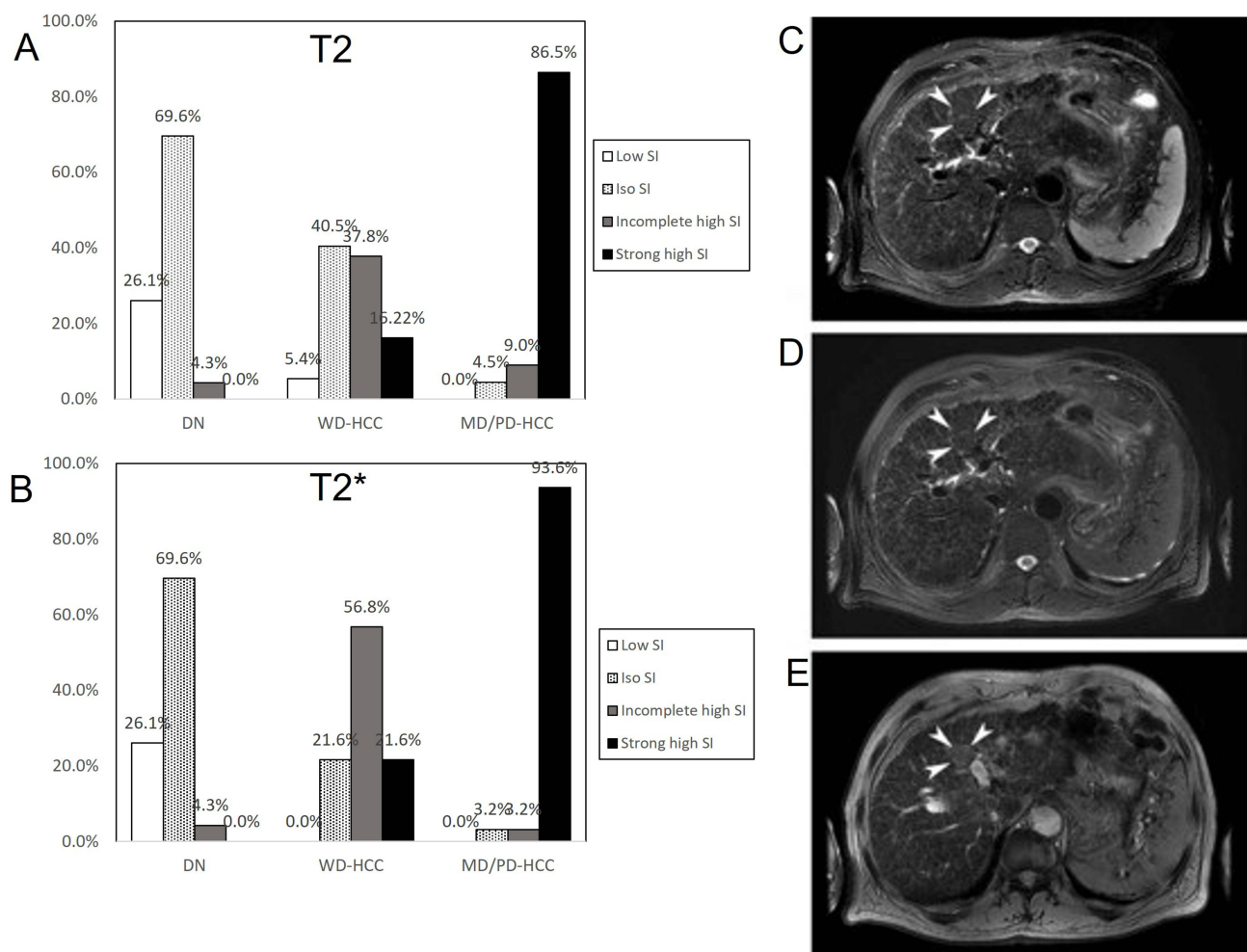

Figure 1 (A and B) Enhancement features of SI in DNs, WD-HCCs and MD/PD-HCCs on IONPs-enhanced T2-weighted images (A) and T2*-weighted images (B). (C–E) A 56-year-old male with WD-HCC proved pathologically. The fat-suppressed T2-weighted imaging (C) and IONPs-enhanced fat-suppressed T2-weighted imaging (D) show an iso SI nodule (arrowheads). The nodule shows incomplete high SI (arrowheads) on IONPs-enhanced T2*-weighted imaging (E). Reprinted with permission from Park HS, Lee J-M, Kim SH, et al. Differentiation of well-differentiated hepatocellular carcinomas from other hepatocellular nodules in cirrhotic liver: value of SPIO-enhanced MR imaging at 3.0 Tesla. *J Magn Reson Imaging*. 2009;29(2):328–335. Copyright © 2009 Wiley-Liss, Inc.[7]

displaying incomplete high SI and thus being diagnosed correctly in T2*-weighted imaging (Figure 1E). Therefore, various hepatocellular nodules showed characteristic imaging features on IONPs-enhanced T2* image.

Since early 1990s, IONPs have been approved to enhance MRI imaging of liver parenchyma. For cancer diagnosis, IONPs are able to enlarge the contrast between tumor tissue and normal liver parenchyma. However, false-negative results might occur for a minority of liver tumors with apparently lower SI than liver parenchyma. IONPs are more suitable for patients with poor renal function compared to Gd-based contrast agents.[41] Additionally, for radiofrequency ablation of liver cancer, which requires sustained tumor visualization during all treatment sessions, IONPs are more readily accessible without the need of additional administration.[41,42] The application of IONPs-enhanced imaging in guiding cancer care is still being explored.[43]

IONPs could convert from functioning as T2 contrast agents to T1 contrast agents when the size is less than 5 nm. Taking advantages of the local micro-environment in tumor site, including lower pH, higher redox pressure and varying enzyme activity, IONPs can be designed to act as stimulus-sensitive nanoprobes, which have small particle size outside the tumor tissue but become larger after entering the tumor tissue, thereby switching from T1 to T2 contrast modes and enhancing the image contrast between the tumor site and the surrounding tissues.[44] In addition, the ultra-small size in circulation could help more permeation, extravasation and accumulation of IONPs into tumor tissue through EPR (enhanced permeability and retention) effect. On the other hand, and the conversion to larger size after entering tumor could help less intravasation back into circulation and more retention of IONPs in tumor.

In one study, ultra-small and small IONPs were designed and injected to orthotopic 4T1 tumors beared mouse.[45] It was found that ultra-small IONPs (3 nm core size) could be detected in interstitial space as far as 60–80 μm from the vessel, while only 10 μm for general IONPs (20 nm core size). The accumulation of IONPs in tumor tissue interstitial was 1.6-fold higher for 3 nm-sized IONPs than that for 20 nm-sized IONPs. Zhang et al synthesized GSH-responsive IONPs with 3.9 nm core size.[46] After intravenous injection of responsive IONPs, the T1 signal in the intracranial tumor was detected readily at 1 h, max at 3 h and still identifiable at 9 h. The T2 signal was detectable at 1.0 h, reached a plateau between 3 h and 5 h, and increased again at 7 h. In comparison, the irresponsive IONPs modified with only targeted ligands fail to visualize the tumors. In summary, ultra-small IONPs are able to enhance passively targeted imaging of tumor tissues and thereby are helpful for precise diagnosis. However, the stimuli-responsive contrast agent needs to remain stable even under diluted conditions but makes structural changes once exposed to bio-stimulation. The fabrication of nanocomposites for spatiotemporally controlled imaging remains a great challenge. In addition, given the heterogeneity across different cancers and their microenvironments, the application of switchable T1-T2 contrast agents needs to be further investigated.

Guiding Sentinel Lymph Node Characterization and Dissection

Lymphatic metastasis plays an important role in the spread of some cancers, such as prostate cancer, breast cancer, melanoma, etc. Sentinel lymph nodes (SLNs) are the first few lymph nodes (LNs) in the pathway of lymphatic drainage from a primary tumor site. Since lymph flow is directional, information about LNs staging and metastasis risk acquired by SLNs dissection and biopsy is extremely important for surgeons to decide whether further surgery should be planned or not.[47] If SLNs do not contain cancer cells, it denotes that the cancer has not yet spread to any other part of the body. As opposed, it probably means a downgrading of prognosis and extended LNs dissection is needed. Generally speaking, SLNs are intraoperatively detected using a gamma probe after injection of ^{99m}Tc (a radioactive tracer) or through visual identification with injected dyes (eg, methylene blue and carbon nanoparticles suspension), or a combination of these two methods.[48,49] Nevertheless, due to several drawbacks, such as ionizing radiation and the dependence on nuclear medicine facilities, the use of ^{99m}Tc is limited to only some regions and institutions. While for blue dye and carbon nanoparticles suspension, they may provoke allergic reactions in some patients.[50]

Small IONPs (15–50nm) display prolonged circulation time and have more possibility to extravasate into surrounding tissues over time after interstitial injection. Once entering into the peripheral tissues, IONPs would be degraded or cleared by lymphatic vessels and eventually end up in macrophages inside SLNs, resulting in magnetically marking of SLNs.[14] Some lymphophilic IONPs, such as Magtrace (brand name, previously Sienna) and Ferucarbotran, have potential to provide viable alternatives to ^{99m}Tc tracer in SLNs mapping and guide surgeons on resection of

SLNs.[8,51] After administration of IONPs, the location of SLNs can be achieved by using some detection techniques, such as the application of handheld magnetometer (eg, Sentimag), MRI, combination of magnetometer and MRI or PET/MRI dual-mode imaging.[52,53] As a negative contrast agent, the IONPs inside normal SLNs can cause remarkably low SI and display a dark area in T2/T2*-weighted MRI. Compared with normal SLNs, there is a decreased number of macrophages along with less phagocytic activity in metastatic LNs, where normal stroma cells are replaced by tumor cells, leading to brighter contrast image than non-metastatic LNs.[54,55]

Several studies have confirmed the non-inferiority of IONPs guided SLNs dissection with handheld magnetometer against ^{99m}Tc-guided SLNs dissection.[50,56,57] In the SentimagIC trial, the combination of IONPs (Sienna) and Sentimag was compared with ^{99m}Tc labeled colloid plus isosulfan blue dye in early-stage breast cancer. The SLNs detection rate was 94.3% (348/369) and 93.5% (345/369) for IONPs and dual tracer (^{99m}Tc plus isosulfan blue dye), respectively.[56] In the 146 patients, the dual tracer identified 98.6% (144/146), and IONPs identified 99.3% (145/146) of the analyzable SLNs. For 25 positive SLNs in 22 patients, 24 were identified by either IONPs or dual tracers.[56]

Despite minimal invasion, ^{99m}Tc and magnetometer guided SLN biopsy are still associated with lymphoedema and pain. IONPs-enhanced MRI with high spatial resolution (<5mm) could improve the discrimination of micro-metastatic SLNs from healthy ones by detecting contrast patterns of SI.[58] Thus, exempting those patients without LNs metastasis from suffering complications following SLNs biopsy.[55,59] In one clinical trial, Motomura et al revealed that metastatic SLNs and even some equivocal situations, such as micro-metastasis and SLNs surrounded by fatty hilum and small vessels, were efficiently identified using Ferucarbotran-enhanced MRI (Figure 2). According to the results of pathological examination,
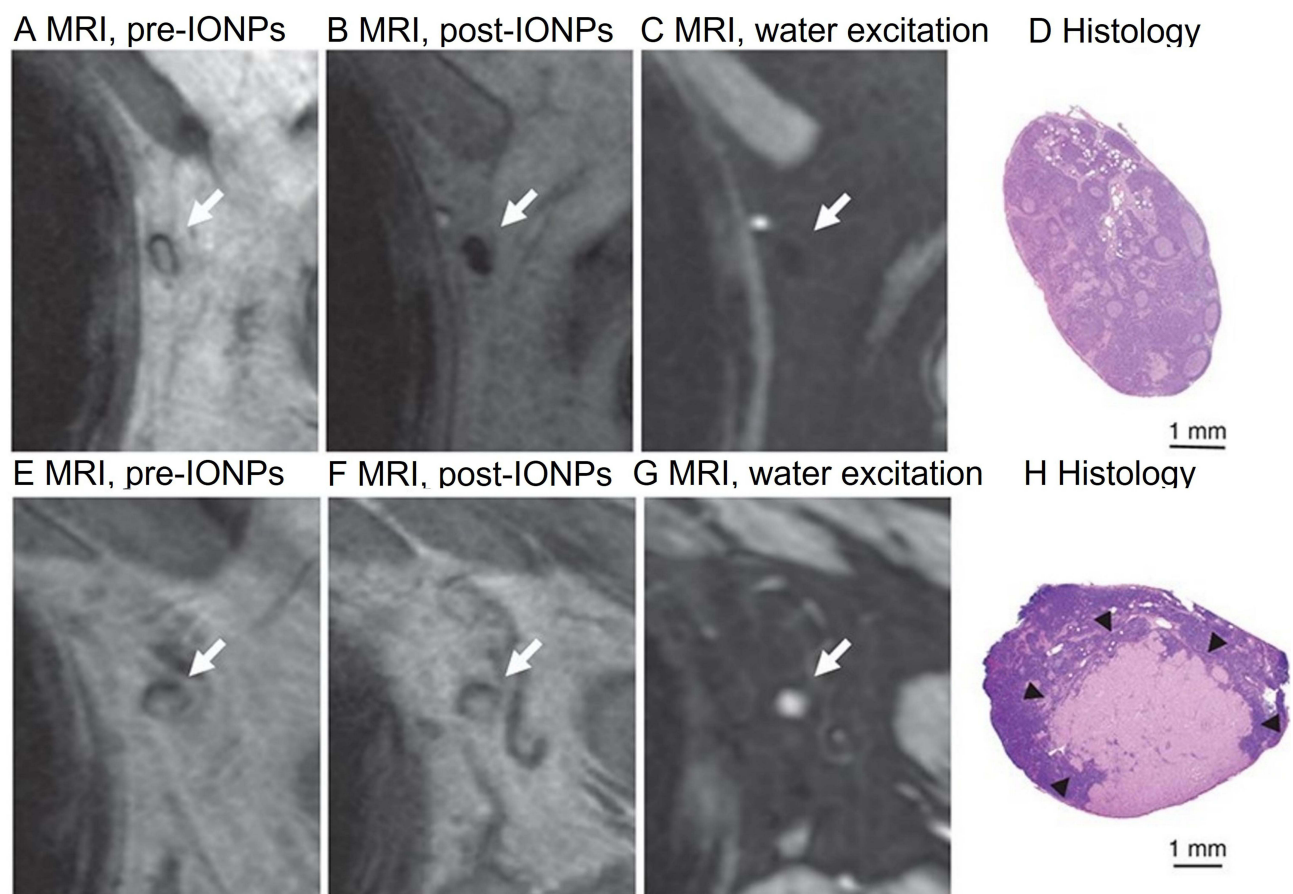

Figure 2 MRI images of (**A–D**) non-metastasis SLNs and (**E–H**) metastasis-positive SLNs. (**A** and **E**) T2*-weighted axial MRI displays SLNs (arrows) before administration of IONPs; the SLNs demonstrate high SI. (**B**) On post-IONPs MRI, the SLNs with homogeneous low SI are diagnosed as benign lesions (arrow). (**F**) The SLNs with a focal area of high SI are considered to be malignant (arrow). (**C**) On water excitation sequence MRI, homogeneous low SI indicates benign SLNs (arrow). (**G**) The enhanced focal area of high SI indicates malignant SLNs (arrow). (**D** and **H**) Pathological analyses confirmed (**D**) benign SLNs and (**H**) malignant SLNs, which are consistent with the imaging findings of (**C** and **G**). Adapted with permission from Motomura K, Izumi T, Tateishi S, et al. Superparamagnetic iron oxide-enhanced MRI at 3 T for accurate axillary staging in breast cancer. *Br J Surg*. 2016;103(1):60–69, copyright 2016 *British Journal of Surgery*.[8]

Ferucarbotran-enhanced MRI accurately identified 94.8% (91/96) SLNs, with the diagnosis sensitivity (positive detection rate) and specificity (negative detection rate) of 95.5% (21/22) and 94.6% (70/74), respectively.[8] Therefore, IONPs-enhanced imaging has great potential to replace SLN biopsy. Besides, IONPs-enhanced MRI could also offer the surgeon an expanded lymphadenectomy template and a roadmap by preoperatively characterizing the distribution of draining SLNs,[60,61] which could gain additional diagnostic value for SLNs beyond the borders of extended LNs dissection.[60,62,63] Winter et al guided SLNs dissection using a combined preoperative MRI and subsequent intraoperative magnetometer following intraprostatic IONPs (Sienna) injection.[63] The combined method had 2.8% additional diagnostic value and identified an unexpectedly high number of SLNs, especially outside the extended SLNs template.

As a complementary technique to MRI, PET could greatly meliorate SLNs detection and enhance the characterization of SLNs status. PET/MRI is an advantageous combined imaging method, especially for cancers with deep-tissue draining lymphatics or variable location of the primary site (eg, melanoma and visceral tumors).[64] In a study including 10 patients, there were one false-positive patient for MRI and one false-negative finding for FDG-PET, respectively. Encouragingly, an overall accuracy of 100% was achieved for the combination of IONPs-enhanced MRI and FDG-PET.[65]

In addition to being free of radiation, IONPs guided by SLNs resection also enjoy several other advantages over radioactive ^{99m}Tc. First, the use of IONPs facilitates preoperative preparation and slightly shortened operating time from probe usage to SLNs removal, thereby allowing for cost reduction and reducing patient discomfort.[66] Second, unlike radioisotope with short half-life (~6h), Sienna has been reported to be easily detectable in LNs up to 27 days post-injection, allowing more flexible time for Sienna injection and second-stage SLNs resection.[67] Third, it is difficult to differentiate SLNs in the periprostatic, presacral, and perirectal areas for prostate cancer because of the interference of high excretion of radiotracer in the bladder. In contrast, no intact IONPs could be found in the urinary tract and the minimal urinary iron excretion in the bladder would not interfere in SLNs detection for prostate cancer.[62,63]

As discussed above, IONPs guided SLNs characterization and dissection have great potential in clinical cancer diagnosis and personalized treatment alone or with other theragnostic. However, lymphatic obliteration in advanced and high-risk tumors could cause invisibility of SLNs, which may hinder the application of SLN dissection. When the lymph pathways are blocked, the afferent lymph will be redirected to other LNs, thus generating false-negative result.[56,63,68] The size and shape of magnetic IONP core, the concentration of IONPs, thickness of adipose tissue surrounding SLNs, the composition of tumor tissue, etc. can influence the signal intensity and the final detection results.[63] In clinical applications, the type and dose of contrast agent should be determined carefully in order to ensure the reliability of this method. In the near future, it can be expected that optimized IONPs with improved relaxation properties and novel detection technique or equipment, such as magnetometer with high resolution (eg, magnetic tunneling junction techniques) will further increase the accuracy of intracorporeal identification of SLNs and guide the subsequent surgery.[57,62,63]

Guiding Hyperthermia Therapy as MPI Tracer

IONPs-based magnetic hyperthermia (MH) is a new technique to kill cancer cells by releasing heat to tumor micro-environment at any tissue depth under alternative magnetic fields. However, it is difficult to selectively actuate quantitative heating of IONPs only in malignant tumors, while sparing surrounding healthy tissues. MPI is a prospective method to directly detect the accumulation rate and quantify the precise thermal dose of IONPs in tumor site. The physics underlying MPI is a gradient magnetic field, which is also present during MH.[22] In addition, the same IONPs excited to generate heat for MH could also be used as tracers in MPI, thus giving MPI the ability for real-time guidance and quantitation of the heating process.[21] With MPI gradient field in place, both MPI signal and heating could be only focused to the FFR.[69] Hence, MPI could guide gradient magnetic field to selectively and quantitatively heat IONPs only in tumor site while minimizing collateral heat damage to surrounding healthy tissues.[70] Additionally, MPI can as well predict the absorption rate and estimate generated heating from the image so that thermal dose planning could be easily performed via monitoring the MPI image intensity.[22,71] In fact, IONPs could be regarded as theranostic nanoparticles, which can generate real-time feedback signals (Figure 3A). The signals between MPI and MH are conducive to gain refined, safe therapy and ultimately improve the patients' outcomes.[21]

Several in-vivo and ex-vivo studies have demonstrated the efficacy of MPI-guided MH therapy. Hensley et al described the construction of a combined MPI-MH system, for which the instruments for MPI and MH were integrated
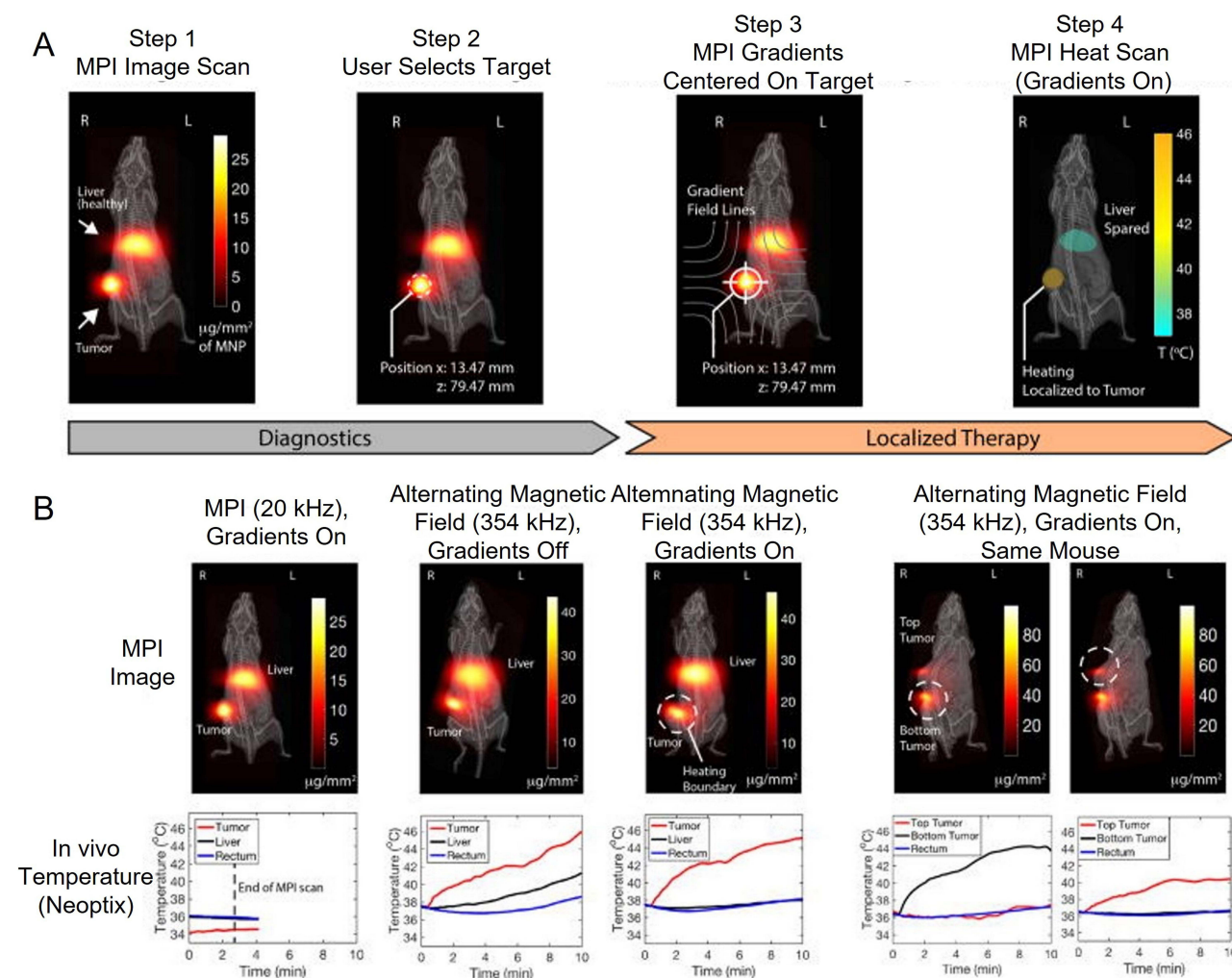
Figure 3 (**A**) Experimental demonstration of theranostic workflow on a U87MG xenograft mouse model with IONPs accumulated in the liver and subcutaneous tumors. Step 1: The biodistribution of IONPs in liver and subcutaneous tumor are clearly visualized with MPI at 20 kHz, 20 mT, which can ensure that heating of IONPs do not happen. Step 2: An area of the subcutaneous tumor is selected to localize MH. Step 3: The MPI gradients are shifted to ensure that FFR are focused on the tumor site. Step 4: With MPI gradients held in position, heat is performed at 354 kHz, 13 mT and only experimentally localized in the FFR (centered at tumor), which can minimize collateral heat damage to the normal liver tissue. (**B**) In vivo study to demonstrate the localization of MH. All the temperatures were obtained by means of Neoptix fiber optic temperature sensors. For the low frequency (20 kHz) and raster trajectory in the process of standard MPI scan, the observed heating of the mouse is negligible. Without MPI gradients, high frequency (354 kHz) scan could heat all in vivo locations with IONPs and inevitably damage liver tissue. Once the selected field is in position, the alternating magnetic field would only heat the tumor site without damaging normal liver tissue. Lastly, a mouse with dual tumors was used to demonstrate arbitrary control of the heating target. When the FFR was centered on the bottom tumor, heating was limited to the bottom tumor without damaging the top one. Next, when FFR was shifted over the top tumor, the alternating magnetic field would only heat the top tumor without damaging the bottom one, showing flexible control of the heating position only by transferring the FFR of MPI. Reprinted with permission from Tay ZW, Chandrasekharan P, Chiu-Lam A, et al. Magnetic particle imaging-guided heating in vivo using gradient fields for arbitrary localization 605 of magnetic hyperthermia therapy. *ACS Nano.* 2018;12(4):3699–3713. Copyright 2018 *American Chemical Society.*[22]

into a single device and MPI is performed at MH frequency. The system allows for seamless switching between imaging and heating modes.[72] With the help of MPI, this study demonstrated on-demand selective heating targets separated by only 3 mm, thereby showing the potential of ablating tumor tissues while sparing surrounding tissues.[72] The predicted temperature measured by the MPI agreed well with experimental data, indicating that the MH process could be precisely controlled and monitored by MPI. In another study, Tay et al used very low frequency (20 kHz) for MPI but 354 kHz for MH to remove heating interference in imaging stage.[22] Gradient magnetic field could heat the targeted sites separated by as small as 7mm without heating of the off-target sites in vitro, which is far less than the standard margin thickness in clinical practice. In a mouse model, sequentially arbitrary control of heating location in the targeted tumor was achieved by using MPI gradients (Figure 3B).[22]

Work on combined MPI and MH has just begun, and the development of MPI thermometry in vivo is vital. As a very promising technique, MPI is hopeful to be integrated into the hyperthermia system, thereby achieving precise heating by providing a temperature feedback mechanism for complete thermal dose control. Further investigation should be focused on developing uniform IONPs to obtain good performance for both MPI and MH. In addition, a targeting ligand is preferred to improve delivery efficiency to tumor tissue.[70,71]

Evaluation of the Therapeutic Effect

Guiding Radiofrequency Ablation and Radiotherapy

Thermal ablation, including radiofrequency ablation (RFA) and radiotherapy, is perceived as a standard therapy for early-stage HCC. Nevertheless, the recurrence rate is high because scattered tumor cells may exist near the tumor tissue. In order to reduce recurrence of HCC, an ablative safety margin of >5mm thickness is recommended. Usually, ablative margin (AM) is assessed by comparing the CT images acquired before and after thermal ablation. However, ablated liver tissues are generally surrounded by congestive or inflammatory areas, particularly in acute and subacute phases after thermal ablation. In CT images, the congestive or inflammatory areas may look like residual tumor tissues, which can lead to diagnostic errors.

IONPs-enhanced MRI could simultaneously visualize and identify irradiated liver parenchyma, non-irradiated liver parenchyma and tumor tissues. Specifically, after thermal ablation, Kupffer cells existing in AM area are damaged and unable to excrete IONPs taken in before thermal ablation, thus resulting in excess IONPs deposition and sustained hypointense signals.[73–77] In contrast, functional Kupffer cells in normal liver parenchyma could eliminate IONPs by converting IONPs to free iron ions, making hypointense signals return to normal level as long as there is an adequate time interval between thermal ablation and imaging (eg, 7 days for Ferucarbotran).[74] Therefore, independent of hepatic perfusion changes post thermal ablation, IONPs-enhanced MRI can clearly distinguish AM from both the surrounding non-tumor parenchyma and ablated tumor, not only showing the positional relationship between targeted tumor and liver parenchyma but also estimating invisible ablated area thickness more precisely.[73,78–80]

Several researchers have demonstrated the availability of IONPs-enhanced MRI for evaluation of safe AM and assessment of the therapeutic effect of RFA. For patients with liver cancer, preservation of liver function is conducive to raising quality of life and extending survival. Compared to minimum AM thickness of 5mm estimated by CT imaging, Fukuda et al found that only 2 mm AM was recommended by pre-administrated Ferucarbotran-enhanced T2* imaging to avoid recurrence.[80] Their study also found that no local recurrence was found at 3 years for patients with AM ≥ 2 mm. Hence, MRI with pre-administrated Ferucarbotran is very meaningful for minimizing both local recurrence and additional damage to normal liver tissue by determining the AM precisely. Ferucarbotran-enhanced T2* imaging could also predict local tumor progression after RFA by evaluating the AM states. Koda et al followed up HCC patients treated by RFA after Ferucarbotran administration for 3 years in order to investigate the correlation between AM states and local tumor progression.[73] They found that the cumulative rate of local tumor recurrence in AM (+) nodules (4.4%, 7.6% and 7.6% in 1, 2 and 3 years) was significantly lower than that of AM (0) nodules (13.9%, 33.4% and 41.8% in 1, 2 and 3 years), whose rim was partly discontinuous without tumor protrusion (Figure 4).[73]

For radiotherapy, several studies have also preliminarily showed that pre-administrated IONPs could be used to assess therapeutic outcomes by accurately visualizing AM. In the study by Furuta et al, three groups of tumor-bearing rats were pre-administrated with Ferucarbotran, saline or (and) sham irradiation, respectively. On 7 days after irradiation, T2*-weighted imaging could only visualize the AM in rats of Ferucarbotran group as markedly, well-defined hypointense areas. In addition, decreased tumor size was observed after irradiation for all rats whose well-circumscribed, continuous hypointense rings (ie hypointense AM) fully encompassed the whole solid tumor, ie showed AM (+) state. Therefore, the therapeutic outcome could be evaluated by IONPs-enhanced imaging of the AM state after radiotherapy.[78,79]

Overall, IONPs-enhanced T2*-imaging can assist the optimization of RFA and radiotherapy. Prior to thermal ablation, T2*-hypointensity enables radiation oncologists to easily mark the delineation of irradiated areas. Meanwhile, post-ablation imaging could accurately show whether thermal ablation has been performed sufficiently based on clear AM visualization. According to the imaging results, AM (+) is an indicator of favorable prognosis, whereas additional ablation or careful follow-up is recommended for patients with AM (0) or AM (-).[78,79] Notably, IONPs-enhanced MRI
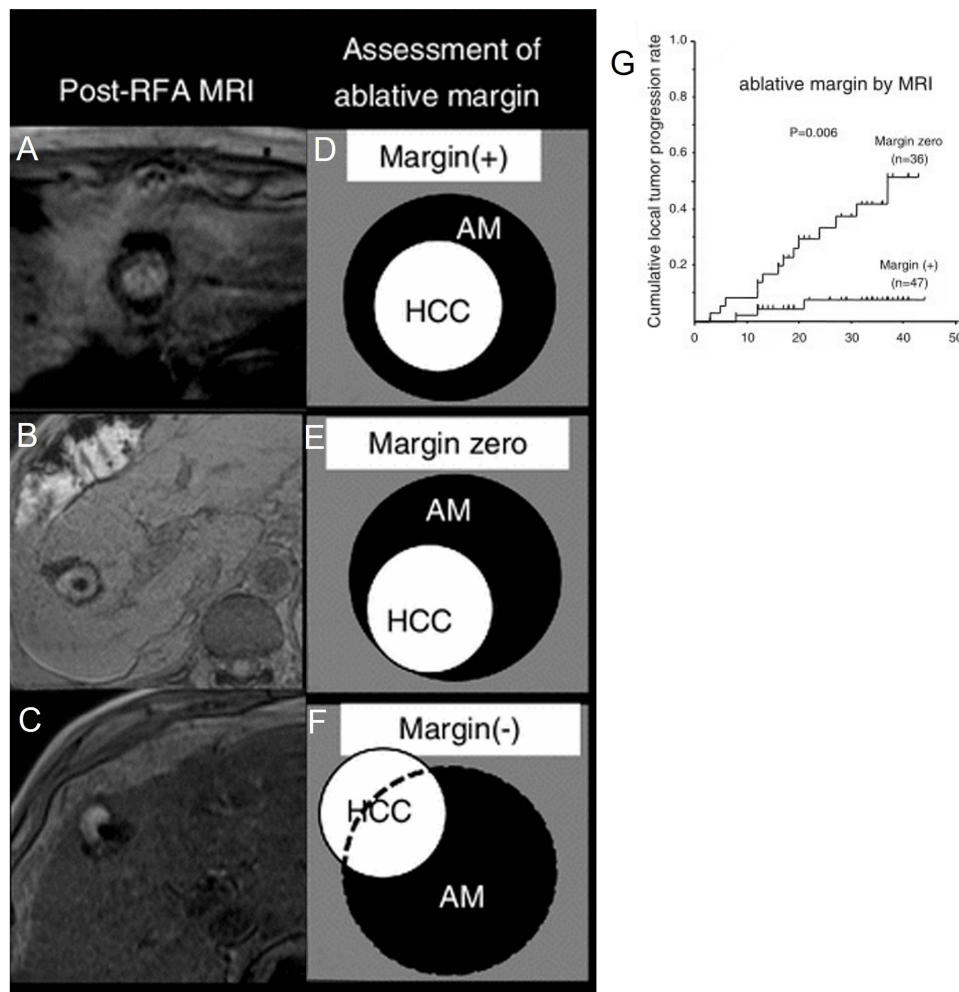
Figure 4 (**A–C**) Three AM images enhanced by pre-administrated IONPs prior to thermal ablation. (**A**) AM (+): the central high-intensity area is completely enwrapped by continuous low-intensity rim. (**B**) AM (0): the central high-intensity area is with partially discontinuous low-intensity rim, but not extend beyond the rim. (**C**) AM (-): the high-intensity area extends out the discontinuous low-intensity rim. (**D–F**) Diagram of three AM states. (**G**) HCC nodules with the state of AM (+) have higher rate of local tumor progression (p = 0.0006) than those with AM (0) according to Kaplan-Meier curve. Used with permission of (SpringerJapanKK) from Koda M, Tokunaga S, Miyoshi K, et al. Ablative margin states by magnetic resonance imaging with ferucarbotran in radiofrequency ablation for hepatocellular carcinoma can predict local tumor progression. *J Gastroenterol.* 2013;48(11):1283–1292. Permission conveyed through Copyright Clearance Center, Inc.[73]

offers distinct superiority over contrast-enhanced CT. Firstly, AM area is displayed clearly in T2* image without the need of comparison with images of other modes. Secondly, T2* imaging of AM area is almost free from influence of post-ablation changes, such as inflammation, congestion and hemorrhage.[73,74,77,80] Thirdly, compared to gadobenate and gadoxetate, which are excreted rapidly from hepatocytes, IONPs allow longer scan window for T2* imaging. Regarding practical applications, emphasis should be given to investigate the reliability of this technique in tumors with different malignancy degrees or clinical stages in animal studies and clinical trials.

Evaluating Anti-Angiogenesis Therapy

Angiogenesis is essential for tumor growth and metastasis by supplying oxygen and nutrients, especially when the tumor volume reaches 1~2 mm^3.[81] Poor prognosis of tumor is closely associated with robust neovascularization and further progression.[82] Antiangiogenic therapy has been proposed as an effective treatment method for malignant tumors since 1970s. Accurate quantification of vasculature is important for post-therapy assessment of antiangiogenic drugs. Vascular characteristics, such as vessel density (VD), blood volume (BV), vessel permeability and blood flow, could reflect vascularization in tumors and the therapeutic response to antiangiogenic drugs.[82–84] Unlike tumor volume, which is a lagging indicator, BV and VD are more sensitive to monitor spatiotemporal progression of tumor vascularization.[82–84]

As a sensitive perfusion MRI approach, susceptibility weighted MRI (SWI-MRI) is a desirable method to quantitatively depict the vascular features by analyzing the MRI signal-intensity time-course for the entire tumor.[85]

Very small IONPs with hydrodynamic diameter <20 nm could partially evade phagocytosis by macrophages and have extended circulation time. In comparison to small molecular Ga chelates, IONPs show slower extravasation from the leaky vessels due to their large size and can act as blood-pool contrast agents.[86] At early time points (several minutes or few hours) after IONPs administration, vessels are shown to have high signal intensity foci in SWI-MRI due to high concentration of IONPs in blood circulation, resulting in a remarkable contrast between intra-tumoral vessels and the surrounding tissues.[87,88] By measuring the dynamic signal change during the passage of IONPs through the vasculature, quantitation of morphological characteristics of vascularization, such as BV and VD, can be obtained through formulas based on a mathematical model.[82,85,87]

Nowadays, IONPs-enhanced SWI-MRI guided angiogenesis measurement has been widely exploited in the treatment of brain tumors.[82,85] It has been revealed that reduced VD closely correlates with the good therapeutic response and the suppressed BV decrease suggests resistance to antiangiogenic drugs.[83] Brain tumor possibly mimics inflammatory diseases because both appear as an expanded area of enhancement in MRI. Due to stress-induced inflammatory response, pseudoprogression after chemoradiotherapy frequently emerges and there is no need to change the treatment paradigm.[89] However, treatment adjustment should be planned if true tumor progression is found. Accordingly, it is of vital importance to differentiate tumor progression from inflammation.[89] Generally, inflammatory lesions usually show relatively low cerebral BV (CBV), whereas glioblastoma progression demonstrates modestly elevated value.[88,89] Based on this recognition, Gahramanov et al tried to distinguish pseudoprogression from tumor progression in patients with glioblastoma multiforme after radiation therapy and chemotherapy with temozolomide using Ferumoxytol-enhanced dynamic SWI-MRI.[9] It was found that quantification of relative CBV (rCBV) with Ferumoxytol alone could successfully distinguish true tumor progression and screen out 100% (9/9) patients who had better prognosis. In contrast, gadoteridol (Gd contrast agent) underestimated the CBV in 50% (5/10) patients with tumor progression (Figure 5).

Compared with common SWI-MRI, steady-state SWI-MRI is more suitable for the imaging of abdominal tumors owing to free of the influence of motion artifacts induced by respiratory and cardiac motions.[87] Kim et al investigated the effectiveness of steady state SWI-MRI with very small IONPs (GEH121333) for measuring tumor responses to bevacizumab in mice bearing subcutaneous TOV-21G human ovarian cancer xenografts.[84] The results showed that BV and VD significantly decreased after bevacizumab treatment, indicating reduced tumor vascularization, which was in agreement with the results of pathological assay.

As a sensitive mean of detecting vascular changes, IONPs-enhanced SWI-MRI has been successfully translated to clinical research.[90,91] Some preclinical and clinical trials have indicated a close relationship between BV/VD and histologic results.[89,90,92] However, the morphological parameters of vessels may not reflect the real growth activity of tumor cells since the metabolic shift could compensate for the reduced vascular supply. Thus, other clinical inspections are still needed to comprehensively and accurately evaluate tumor growth. IONPs-enhanced SWI-MRI guided angiogenesis measurement could offer auxiliary information about the effect of anti-cancer drugs. In addition, despite the larger size against other blood pool agents, extravasation of IONPs into interstitial space still cannot be avoided, which might bring minor interference for inspection. Due to the paradox that IONPs with smaller size have longer circulation but are prone to extravasate from blood vessels more easily, the size of IONPs should be adjusted to achieve an ideal balance between circulation time and extravasation. Therefore, further study is warranted to optimize the evaluation of tumor angiogenesis by IONPs-enhanced MRI in the future.

Detecting Circulating Tumor Cells

CTCs are the scarce tumor cells (1–10 cells/mL) shedding into blood circulation from tumor lesions and constitute the seeds for metastasis. So far, CTCs in bloodstream are confirmed to be a very important indicator for metastasis and recurrence of some carcinomas, such as breast, colon, and prostate cancer.[93–95] Dynamic monitoring of CTCs has proven to have great clinical significance in early diagnosis, predicting PFS and overall survival.[95–97] Moreover, by analyzing the genomic and proteomic profiles of captured CTCs, it is also helpful to estimate the risk of tumor metastasis and facilitate personalized therapy. Since only a small amount of peripheral blood (about 6~8 mL) is needed for CTCs detection, it
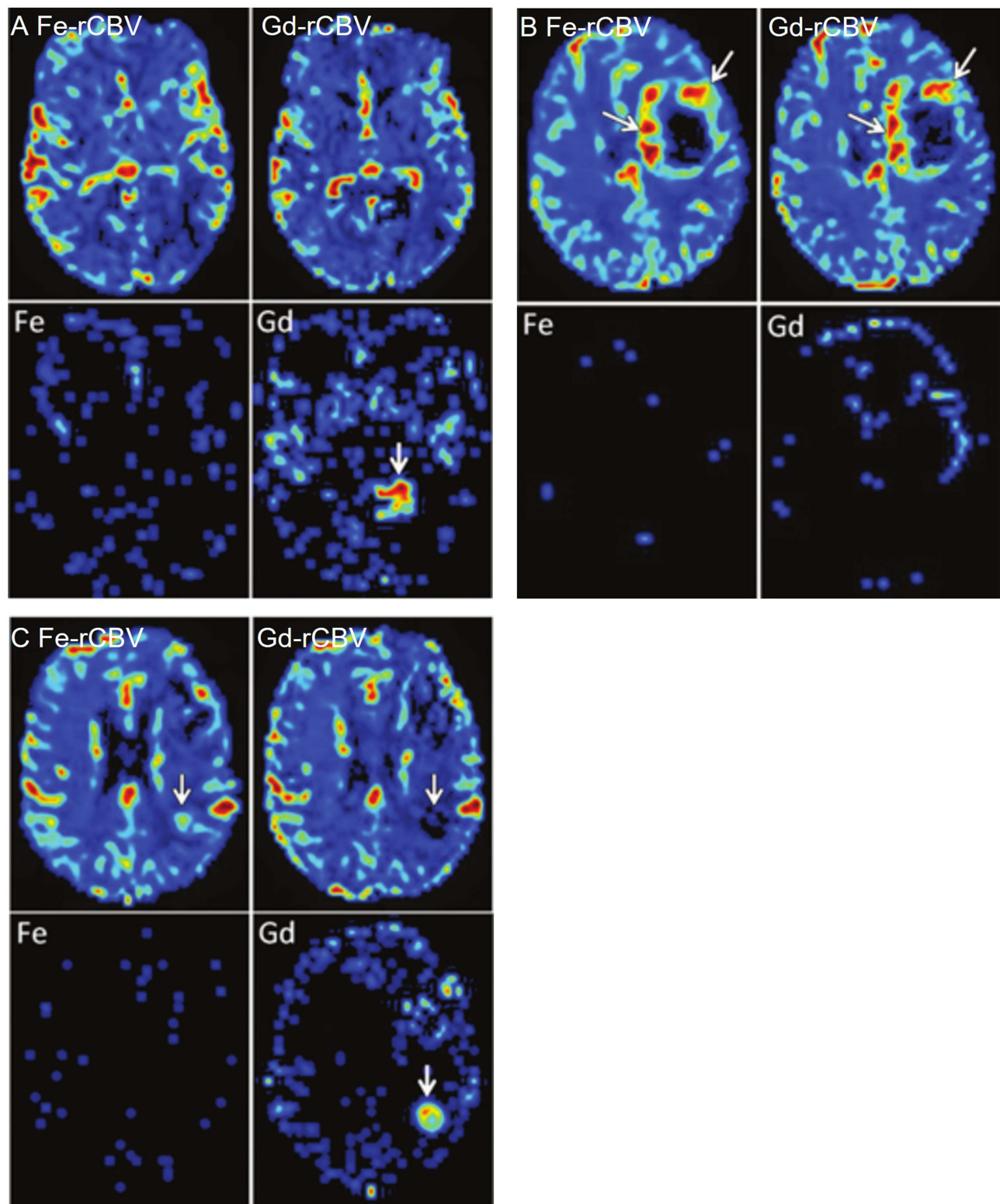
Figure 5 (**A**) Axial images show tumor pseudoprogression for a 73-year-old patient with GBM at 3 months after chemoradiotherapy. Ferumoxytol (Fe-rCBV) and gadoteridol (Gd-rCBV) enhanced SWI-MRI show apparently low rCBV (≤1.75). Leakage maps suggest no contrast extravasation for Ferumoxytol (Fe) and observable contrast extravasation for gadoteridol (Gd, arrow). (**B**) Axial images show true tumor progression (arrow) for a 59-year-old patient with GBM at 2 weeks after chemoradiotherapy. Ferumoxytol (Fe-rCBV) and gadoteridol (Gd-rCBV) enhanced SWI-MRI indicate apparently high rCBV (>1.75). Leakage maps suggest no contrast extravasation for Ferumoxytol (Fe) but small leakage for gadoteridol (Gd). (**C**) For a 68-year-old patient with GBM at 2 weeks after chemoradiotherapy, axial images show discordance between Ferumoxytol (Fe-rCBV) and gadoteridol (Gd-rCBV) enhanced SWI-MRI. High rCBV (>1.75) obtained via Ferumoxytol (Fe-rCBV) enhanced SWI-MRI indicates active tumor (arrow). However, low rCBV (≤1.75) calculated through gadoteridol parametric map (Gd-rCBV) indicates pseudoprogression. Leakage map suggests no contrast extravasation for Ferumoxytol (Fe) but observable contrast leakage for gadoteridol (Gd). Adapted with permission from Gahramanov S, Muldoon LL, Varallyay CG, et al. Pseudoprogression of glioblastoma after chemo- and radiation therapy: diagnosis by using dynamic susceptibility-weighted contrast-enhanced perfusion MR imaging with ferumoxytol versus gadoteridol and correlation with survival. *Radiology*. 2013;266(3):842–852. Copyright 2013 *Radiology*.[9]

enjoys advantages of less invasiveness, convenience in sampling and good patient compliance over traditional diagnostic techniques.[95,97–99]

CTCs can be isolated based on their physical characteristics (eg, size, density, surface charge, etc.) or expression of specific receptors. Due to its excellent magnetic behavior (>40 emu/g) and easy construction, antibody-modified IONPs can be used for magnetic immunization separation and detection of certain cell populations from biological suspensions.[28,99–101] Briefly, modified IONPs can specifically bind to corresponding receptors on the surface of CTCs and thus isolate CTCs in an external magnetic field. Then, CTCs could be detected through FI or micro-MRI technology.[99–101] Attributing to simple and gentle processing, 93.8% of the captured CTCs could preserve their viability and function, thereby enabling in vitro culture and further study.[102]

A CellSearch system using IONPs linked with anti-epithelial cell adhesion molecule (anti-EpCAM) antibodies has been approved by FDA to diagnose colorectal, prostate and breast cancer.[103] However, for a significant fraction of patients, this system may lead to inherently EpCAM-negative and epithelial-to-mesenchymal transition (EMT) inverted CTCs being ignored.[99,100] In order to improve the accuracy of CTCs detection, Chen et al constructed IONPs loaded magnetic immunoliposomes (MIL) linked with one of the four kinds of antibodies (EpCAM, EGFR, HER-2 and mucin-1) (Figure 6A).[28] The results indicated that the cumulative CTCs-positive rate was up to 87.5% with four different magnetic nanoparticles, which is much higher than that of any single magnetic nanoparticles and their mixed counterpart (Figure 6B). After long-term follow-up, PFS rate was lower in patients with CTCs number ≥2 than 0–1, which suggested that CTCs counts may provide useful prognostic information and multi-markers modified fluorescence-IONPs system could be a useful tool for CTCs detection in tumor screening and prognosis evaluation.[28] In another study, a similar conclusion was also drawn that dynamic monitoring of CTCs using fluorescent–magnetic IONPs at 1 day before and 7 and 30 days after natural killer (NK) cells therapy was useful to well assess treatment efficacy and predict prognosis.[96]

Micro-MRI is another effective technology for CTCs detection, which can directly count CTCs by assessing the T2 signal intensity of antibodies modified IONPs.[104] As a robust point-of-care method for identifying scarce cell populations, IONPs-enhanced micro-MRI enables direct CTCs measurement in peripheral blood sample as small as 100 uL without the need for enrichment or subsequent multistep processing.[97,98] Based on the molecular profiling of biopsies from 58 patients, Ghazani et al examined the sensitivity of quad-marker micro-MRI (EpCAM, MUC-1, HER-2 and EGFR) and CellSearch by analyzing the same peripheral blood samples of 15 clinical ovarian cancer subjects. The results showed that CTCs were found in 87% patient (13/15) for quad micro-MRI, while the corresponding result was only 7% (1/15) for CellSearch. In addition, for the only CTCs-positive patient assessed by CellSearch, only 18 CTCs were detected, while 170 CTCs were found by IONPs-enhanced micro-MRI, indicating higher performance for quad-marker micro-MRI versus CellSearch in quantifying CTCs.[98]

IONPs could also be flexibly conjugated with different aptamers of other biomarkers (eg, CD34, fibronectin and nucleic acid). Therefore, it is conceivable to achieve screening and analysis of various CTCs and even circulating DNA with good patient compliance. Despite its great potential, there are still some limitations for IONPs-based imaging in the assessment of CTCs. First, in vitro CTCs detection lacks the ability of cross-sectional imaging to identify tumor sites. Therefore, MRI or CT is necessary to supplement this novel technique. Second, reliable threshold value, which could specifically screen high-risk group and offer guidance on rational therapy, is still lacking. Recent studies displayed that simultaneously detecting and killing CTCs by integrating detection and therapeutic components into one whole magnetic device is of great potential for cancer therapy.[105,106] With the development of more specific biomarkers, high-performance IONPs and imaging techniques, the clinical applicability of IONPs in CTCs measurement will exert more positive effect to assist cancer treatment decision.

Tracking Therapeutic Cells

Recently, cell therapies have received intensive research attentions in the treatment of multiple diseases and disorders because of their ability to restore, replace or repair damaged tissues.[107] Encouragingly, cell therapies are constantly evolving, improving and providing a new option to cancer patients. To date, hematopoietic stem cell (HSC) transplantation has already gained wide application in treating hematological malignancies for decades. Adoptive cell therapy, including chimeric antigen receptor T cell (CAR-T), T cell receptor engineered T cell (TCR-T) and NK cell, is
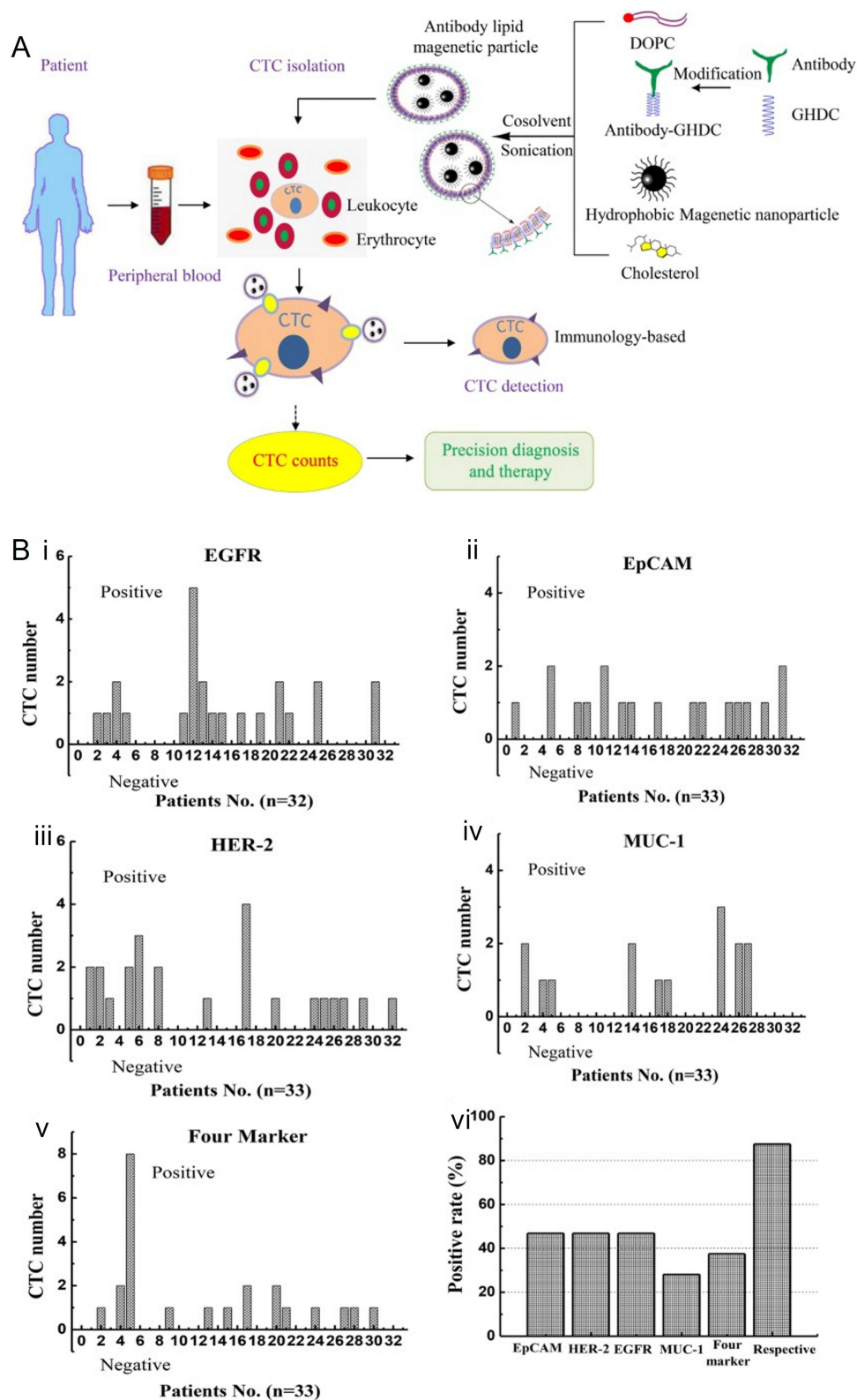
Figure 6 (**A**) The diagrammatic sketch of magnetic immunoliposome preparation and CTC detection. (**B**) CTC numbers detected by different magnetic nanoparticles, (i) EGFR, (ii) EpCAM, (iii) HER-2, (iv) MUC-1 and (v) mixture of four magnetic nanoparticles; (vi) CTC positive rate of the 32 patients. Adapted with permission from Chen J, Chen L, Du S, et al. High sensitive detection of circulating tumor cell by multimarker lipid magnetic nanoparticles and clinical verifications. *J Nanobiotechnology*. 2019;17 (1):116. doi:10.1186/s12951-019-0548-1. Copyright 2019 *Journal of Nanobiotechnology*.[28]

particularly mighty against many cancers.[108] In addition, stem cells have also been exploited as carriers of anti-cancer drugs owing to their ability to home to and integrate within solid tumors.[109] Thus, cell therapies hold great promise for promoting advances in cancer management.[110]

In principle, the therapeutic effects of engrafted cells depend on the migration, proliferation and function of injected cells.[111] Accordingly, tracking and monitoring of therapeutic cells after transplantation is absolutely necessary for a comprehensive understanding of their biological fate and therapeutic process in vivo.[112] Several molecular imaging modalities can be used for cell tracking, such as optical imaging represented by bioluminescence imaging (BLI) and FI, nuclear imaging represented by MRI and PET as well as single-photon emission computed tomography (SPECT).[110,113] Due to long-term stay in cells and rapid acquisition of images, IONPs are one of the most preferred options for cell tracking both in preclinical and clinical studies.[112]

Adoptive CAR-T immunotherapy has shown high effectiveness in hematological tumors. Unfortunately, its therapeutic efficacy in solid tumors is controversial. In order to supervise the infiltration and persistence of CAR-T cells within solid tumor tissues, Xie et al labeled EGFRvIII and IL13Rα2 targeting CAR-T cells with IONPs at 37.5 Fe μg/mL and monitored their kinetic behavior in glioblastoma.[114] After injection, 7.0-T MRI images showed an increase in spot-like signals from 3 days to 14 days within tumor parenchyma, suggesting existence of labeled CAR-T cells, which was further confirmed by pathological staining. Compared to PBS and IONPs loaded T cells, the mice treated with IONPs loaded CAR-T cells exhibited slower tumor growth and prolonged survival (Figure 7). Furthermore, the therapeutic efficacy was concurrent with the appearance of increasing signals. Therefore, IONPs-enhanced MRI was able to sensitively track the labeled CAR-T cells and evaluate their therapeutic response. In another study, ferumoxide was used to label dsRed (a red fluorescent protein) expressing HSC. The result showed that ultra-high-field MRI (17.6 T) can visualize the remodeling
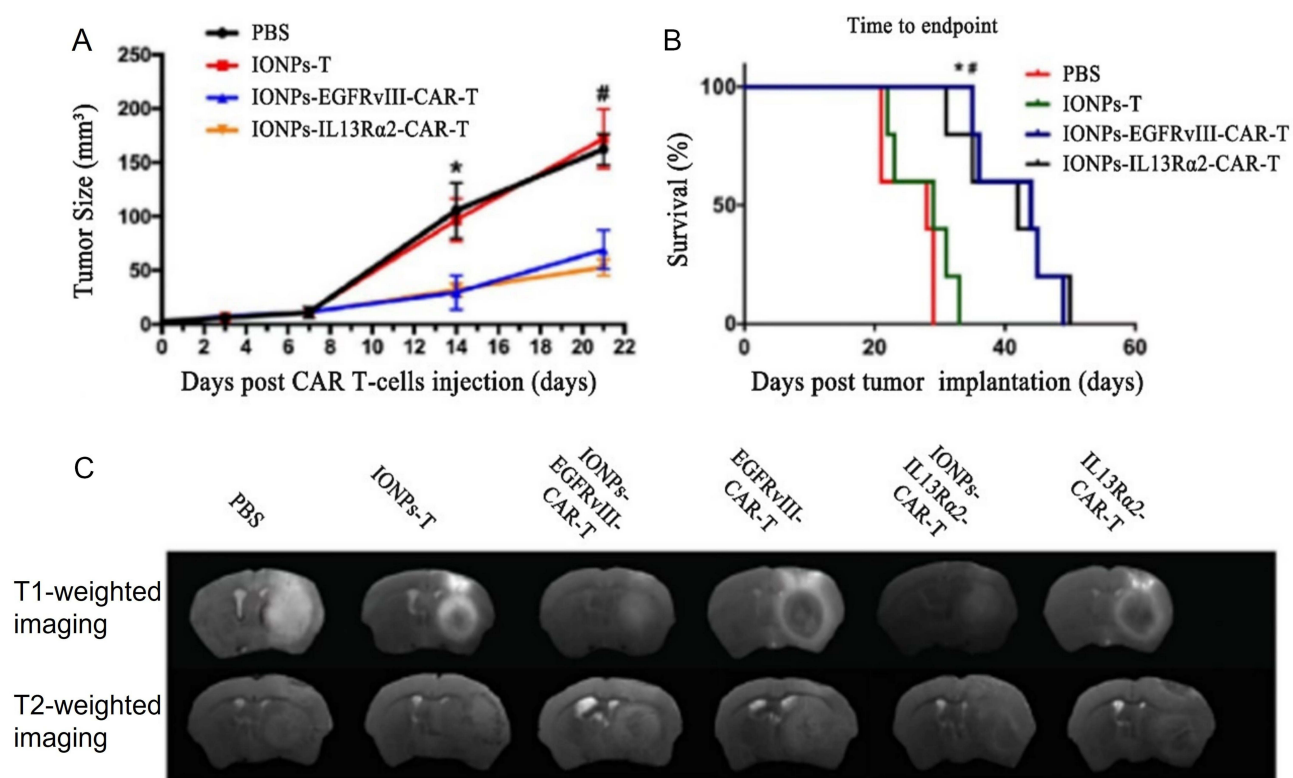

Figure 7 Monitoring of the treatment response to IONPs labeled CAR-T cells via perfusion and diffusion MRI. (**A**) Tumor growth curves based on MRI images, indicating significant differences on day 14 and day 21 after treatment. *P < 0.05, IONPs-CAR-T cell group versus PBS and IONPs labelled T cell groups on day 14. #P < 0.05, IONPs-CAR-T cell group versus PBS and IONPs-T cell groups on day 21. (**B**) Kaplan–Meier curve of survival rate. *P < 0.05, IONPs labelled GFRvIII-CAR-T cell group versus IONPs labelled T cell and PBS groups. #P < 0.05, IONPs labelled IL13Rα2-CAR-T cell group versus IONPs labelled T cell and PBS groups (n = 5). (**C**) Representative axial T2-weighted images (lower row) and T1-weighted imaging (upper row) on day 3 after CAR-T cell injection. Adapted from *Cytotherapy*, 23(3), Xie T, Chen X, Fang J, et al. Non-invasive monitoring of the kinetic infiltration and therapeutic efficacy of nanoparticle-labeled chimeric antigen receptor T cells in glioblastoma via 7.0-Tesla magnetic resonance imaging. *Cytotherapy*. 211–222. Copyright 2021, with permission from Elsevier.[114]

of bone marrow caused by high dose of radiation or chemotherapy with high-resolution of images ($28 * 28 * 60 \ \mu m^3$) in live mice and allow visualization of iron-labeled cells in real time, which allow fully validated longitudinal analysis of cell fate and thus stimulate improvement of HSCT.[115]

To some extent, clinical translation of IONPs-based imaging for monitoring therapeutic cells was hindered by low sensitivity and tracer dilution. To solve this problem, combined imaging techniques could provide more comprehensive information in terms of location and cell viability. Thin et al achieved tri-modal imaging capabilities by incubating luciferase-expressing human adipocyte-derived stem cells (ADSCs) with Indium-111 radio-labelled IONPs. After intravenously or intracardially administration of ADSCs to orthotopic breast tumors engrafted mice, in vivo process of ADSCs was monitored by IONPs-based MRI, luciferase-based BLI and Indium-111 based SPECT, respectively. The results indicated that ADSCs could be observed as early as 1-h post intracardial injection and the percentage of ADSCs within tumors was twofold higher than that through intravenous injection. Therefore, this tri-modal imaging technique was able to evaluate the number of stem cells delivered to tumors and compare the efficiency of different administration routes, thus optimizing stem cell-based cancer therapies.[109]

IONPs-based imaging for cell tracking still faces some challenges, such as relatively low sensitivity, tracer dilution upon cell division and interference of false-positive results arising from the release of the labelling agents from the dead cells or subsequent uptake by phagocytic cells.[116] With the rapid development of multimodal molecular imaging technique, IONPs-based imaging approach will greatly facilitate the future development of cell-based therapy.

Promotion of Nanomedicine Development

Nanomedicines are nanoscale preparations by encapsulating therapeutic drugs into liposomes, polymer nanoparticles, micelles, etc.[117] The size of nanomedicines for cancer therapy typically spans from 5 to 200 nm. Compared to small-molecular chemotherapeutics, nanomedicines have more favorable pharmacokinetic characteristics, including passive targeting of tumor sites and prolonged drug exposure, thus increasing therapeutic effect and reducing side effects. Although tremendous researches have been conducted in past decades, only a small minority of nanomedicines have successfully obtained marketing approval, such as liposomal doxorubicin, albumin-bound (nab)-paclitaxel, etc. Two reasons mainly account for the poor clinic translation:[117] (i) stable manufacturing technique for the relatively complicated formulation of nano-preparations is lacking, leading to poor batch-to-batch reproducibility. (ii) the excellent therapeutic effect observed in preclinical models could be hardly reproduced in clinical trials, partially due to the fact that the notable EPR-mediated specific accumulation of nanodrugs in tumors observed preclinically is rather modest in clinical reality. In fact, the preclinical mouse models are highly homogenous because the inoculated tumor xenografts are all part of the same sub-clone.[118] However, various tumors in the real world are highly heterogeneous.

It is generally considered that the EPR effect dramatically varies across different individuals with the same tumor type and even over time during tumor development.[119] Therefore, effective assessment of variable EPR effect by visualizing and quantifying the nanomedicine accumulation in tumor tissue before nanomedicines treatment is meaningful.[118] Alike in particle size, IONPs could behave in similar pharmacokinetic behavior and achieve colocalization with nano-formulations in perivascular areas.[120,121] Miller et al found that ferumoxytol could predictably demonstrate colocalization areas for PLGA-PEG nanoparticles with accuracy >85% in the tumor microenvironment.[120] Therefore, IONPs-enhanced quantitative MRI can be applied to monitor tumor targeting ability of nanomedicine and thus identify sub-population with higher likelihood of drug response in a straightforward and cost-effective way.

In most cases, IONPs can act as companion nano-diagnostics to facilitate the research of nanomedicines.[119] Depending on MRI signal intensity and pathological examination, it has been found that the deposition of the companion IONPs and nanotherapeutics in the target site correlate well.[118,119,121] Ramesh K. Ramanathan found a highly hetero-geneous EPR effect in solid tumors among different patients by calculating the accumulation of ferumoxytol in tumor lesions according to R2* signal intensity standard curve of ferumoxytol. Then, the patients received liposomal irinotecan and subsequent biopsy examination at 72 h. The results indicated that the accumulation levels of ferumoxytol and irinotecan were significantly related. Moreover, patients with higher ferumoxytol accumulation showed a larger reduction in tumor lesions compared to those patients with below-average accumulations of ferumoxytol.[121] In another animal experiment, Chen et al assessed the EPR effect by measuring tumor/normal tissue T2* signal ration (TNR value) of
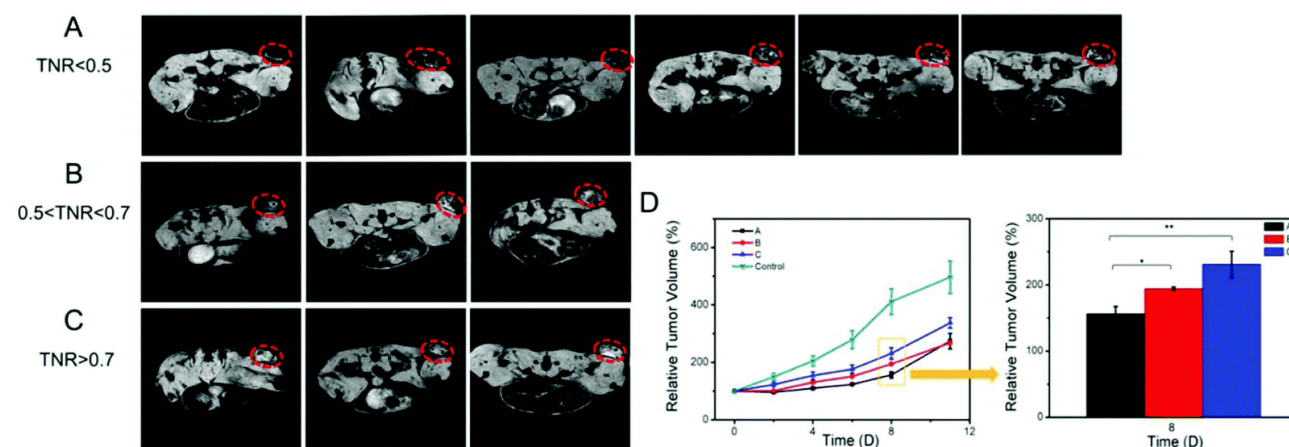
Figure 8 (**A–C**) T2* images of 12 mice tumors obtained 3h post-injection of IONPs using 7T MRI scanner. Tumor site is showed by the red dotted line. The mice were divided into 3 groups depending on TNR values. Mice in A, B and C groups were injected with paclitaxel micelle with a single dose of 60 mg/kg/day on 0, 4th and 8th day. (**D**) Tumor volume change. The data are shown as mean ± SE and the asterisk indicated statistical significance (*p < 0.05, **p < 0.01). Used with permission from RSC Pub. Chen L, Zang F, Wu H, et al. Using PEGylated magnetic nanoparticles to describe the EPR effect in tumor for predicting therapeutic efficacy of micelle drugs. *Nanoscale*. 2018;10 (4):1788–1797. Permission conveyed through Copyright Clearance Center, Inc.[119]

IONPs-based on the fact that the smaller TNR values indicate more IONPs accumulation in tumor site. In the following study, it was found that the mice with TNR < 0.5 exhibited optimal inhibitory effect as compared to those with 0.5 < TNR < 0.7 and TNR > 0.7 after intravenous treatment with paclitaxel micelles.[119] These results revealed high potential of IONPs-enhanced MRI to accurately evaluate the EPR effect and predict the therapeutic efficacy of nanomedicines (Figure 8).

Co-encapsulating IONPs and therapeutic drugs within a single nano-formulation, ie nano-theranostics, is another way to obtain information on the biodistribution of nanodrugs in vivo.[118] Due to their strong interaction with therapeutic agents and inherent imaging ability, IONPs are intrinsically especially suitable for theranostic purposes.[122–124] Pan et al developed doxorubicin and IONPs co-entrapped micelles for the treatment of folate receptor over-expressed breast cancer.[125] In MRI images, mice treated with folic-acid targeting doxorubicin-IONPs micelles displayed a larger hypointense presence in tumor site at 12 and 36 h than non-targeting micelles, indicating a higher nanodrug distribution. The tumor growth curves of xenografted mice with the treatments for 24 days showed greater antitumor effectiveness of targeting micelles than non-targeting micelles, which may be associated with differentiated micelle accumulation. In another study by Zheng et al, similar result was also observed that MRI signal could reflect the tumor accumulation of paclitaxel-IONPs coloaded liposomes and predict their antitumor efficacy. Hence, the targeting ability of nanomedicines in tumor tissues could be clearly demonstrated with theranostics-enhanced MRI.[124]

In summary, IONPs-enhanced MRI holds great promise to select patients with high EPR characteristic for nanotherapeutics and predicts the therapeutic response, thus providing a major stepping stone toward clinical translation.[118] However, combined nano-theranostics is rare in clinic, because of substantial cost challenges and strict regulations for clinical trials.[118,126] In addition, the clinical application of combined nano-theranostics with good reproducibility may also be hindered by complex construction. In comparison, companion diagnostic approach enjoys advantages of versatility and clinical accessibility, depending on the highly consistent distribution of IONPs and nano-medicine. Until now, most of these researches are restricted to animal models. For more extensive application, further clinical investigations are required to examine the correlation between various nanomedicines distribution and long-term efficacy of IONPs-based medical imaging.[123]

Conclusions and Future Prospects

In summary, the broad application of IONPs-based medical imaging in many aspects of cancer management is reviewed. IONPs-based medical imaging has been successfully applied to visualize malignant tumor lesions, evaluate AM after RFA and radiotherapy, locate and characterize the state of SLNs, act as MPI agents to guide MH in real time, as well as

observe morphological imaging of tumor vasculature and longitudinally assess antiangiogenic therapy. IONPs could also be applied as isolating or labeling agents to detect scarce CTCs or trace therapeutic cells in vivo, so as to provide reference for personalized cancer therapy. In addition, with similar nanoscale size, IONPs are also able to accelerate the development of nanomedicines by estimating their distribution in tumor sites.

There is a bright future for the application of IONPs in cancer care. After several initial frustrations, in which Ferucarbotran and Ferumoxide were initially marketed and later withdrawn (due to better alternatives for diagnostic applications), many different (pre-)clinical directions involving the application of IONPs are being explored.[14] With the development and maturity of new imaging technique (such as MPI and ultrasmall IONPs enhanced MRI) and cancer care concepts (CTCs detection), IONPs-based imaging can further promote the diagnosis and therapy of tumor patients. Encouragingly, as a new research technique, IONPs based imaging is able to help to understand the biodistribution and estimate the efficacy of investigated medicines. In spite of tremendous potential for IONPs-based imaging in tumor field, additional attempts need to be conducted to demonstrate the cost of industrial production and practicability of clinical transformation. With the development of a new generation of IONPs, novel imaging equipment and technology, IONPs-based medical imaging might add more reformations for both diagnosis and therapy guidance of cancer in the future.

Acknowledgments

Disclosure

The authors report no conflicts of interest in this work.

References

1. Sung H, Ferlay J, Siegel RL, et al. Global cancer statistics 2020: GLOBOCAN estimates of incidence and mortality worldwide for 36 cancers in 185 countries. *CA Cancer J Clin*. 2021;71(3):209–249. doi:10.3322/caac.21660
2. Wu C, Li M, Meng H, et al. Analysis of status and countermeasures of cancer incidence and mortality in China. *Sci China Life Sci*. 2019;62 (5):640–647. doi:10.1007/s11427-018-9461-5
3. Li Y, Zhang. H. Fe$_3$O4-based nanotheranostics for magnetic resonance imaging-synergized multifunctional cancer management. *Nanomedicine*. 2019;14(11):1493–1512. doi:10.2217/nnm-2018-0346
4. Lin S-Y, Huang R-Y, Liao W-C, et al. Multifunctional PEGylated Albumin/IR780/Iron oxide nanocomplexes for cancer photothermal therapy and MR imaging. *Nanotheranostics*. 2018;2(2):106–116. doi:10.7150/ntno.19379
5. Wu W, Klockow JL, Mohanty S, et al. Theranostic nanoparticles enhance the response of glioblastomas to radiation. *Nanotheranostics*. 2019;3 (4):299–310. doi:10.7150/ntno.35342
6. Kato H, Kanematsu M, Kondo H, et al. Ferumoxide-enhanced MR imaging of hepatocellular carcinoma: correlation with histologic tumor grade and tumor vascularity. *J Magn Reson Imaging*. 2004;19(1):76–81. doi:10.1002/jmri.10425
7. Park HS, Lee J-M, Kim SH, et al. Differentiation of well-differentiated hepatocellular carcinomas from other hepatocellular nodules in cirrhotic liver: value of SPIO-enhanced MR imaging at 3.0 Tesla. *J Magn Reson Imaging*. 2009;29(2):328–335. doi:10.1002/jmri.21615
8. Motomura K, Izumi T, Tateishi S, et al. Superparamagnetic iron oxide-enhanced MRI at 3 T for accurate axillary staging in breast cancer. *Br J Surg*. 2016;103(1):60–69. doi:10.1002/bjs.10040
9. Gahramanov S, Muldoon LL, Varallyay CG, et al. Pseudoprogression of glioblastoma after chemo- and radiation therapy: diagnosis by using dynamic susceptibility-weighted contrast-enhanced perfusion MR imaging with ferumoxytol versus gadoteridol and correlation with survival. *Radiology*. 2013;266(3):842–852. doi:10.1148/radiol.12111472
10. Turkbey B, Czarniecki M, Shih JH, et al. Ferumoxytol-enhanced MR lymphography for detection of metastatic lymph nodes in genitourinary malignancies: a prospective study. *Am J Roentgenol*. 2020;214(1):105–113. doi:10.2214/AJR.19.21264
11. Wade TP, Kozlowski. P. Longitudinal studies of angiogenesis in hormone-dependent Shionogi tumors. *Neoplasia*. 2007;9(7):563–568. doi:10.1593/neo.07313
12. Schilham MGM, Zamecnik P, Privé BM, et al. Head-to-head comparison of 68Ga-prostate-specific membrane antigen PET/CT and ferumoxtran-10 enhanced MRI for the diagnosis of lymph node metastases in prostate cancer patients. *J Nucl Med*. 2021;62(9):1258–1263. doi:10.2967/jnumed.120.258541
13. Robinson SP, Howe FA, Griffiths JR, et al. Susceptibility contrast magnetic resonance imaging determination of fractional tumor blood volume: a noninvasive imaging biomarker of response to the vascular disrupting agent ZD6126. *Int J Radiat Oncol Biol Phys*. 2007;69(3):872–879. doi:10.1016/j.ijrobp.2007.06.061
14. Dadfar SM, Roemhild K, Drude NI, et al. Iron oxide nanoparticles: diagnostic, therapeutic and theranostic applications. *Adv Drug Del Rev*. 2019;1(138):302–325.
15. Huang Y, Hsu JC, Koo H, et al. Repurposing ferumoxytol: diagnostic and therapeutic applications of an FDA-approved nanoparticle. *Theranostics*. 2022;12(2):796–816. doi:10.7150/thno.67375

16. Wang G, Zhang X, Skallberg A, et al. One-step synthesis of water-dispersible ultra-small Fe3O4 nanoparticles as contrast agents for T1 and T2 magnetic resonance imaging. *Nanoscale*. 2014;6(5):2953–2963. doi:10.1039/c3nr05550g

17. Jin R, Lin B, Li D, et al. Superparamagnetic iron oxide nanoparticles for MR imaging and therapy: design considerations and clinical applications. *Curr Opin Pharmacol*. 2014;1(18):18–27. doi:10.1016/j.coph.2014.08.002

18. Alvares RDA, Szulc DA, Cheng. H-LM. A scale to measure MRI contrast agent sensitivity. *Sci Rep*. 2017;7(1):15493. doi:10.1038/s41598-017-15732-8

19. Jeon M, Halbert MV, Stephen ZR, et al. Iron oxide nanoparticles as T1 contrast agents for magnetic resonance imaging: fundamentals, challenges, applications, and prospectives. *Adv Mater*. 2020;33(23):e1906539. doi:10.1002/adma.201906539

20. Makela AV, Gaudet JM, Schott MA, et al. Magnetic particle imaging of macrophages associated with cancer: filling the voids left by iron-based magnetic resonance imaging. *Mol Imaging Biol*. 2020;22(4):958–968. doi:10.1007/s11307-020-01473-0

21. Bauer LM, Situ SF, Griswold MA, et al. High-performance iron oxide nanoparticles for magnetic particle imaging - guided hyperthermia (hMPI). *Nanoscale*. 2016;8(24):12162–12169. doi:10.1039/C6NR01877G

22. Tay ZW, Chandrasekharan P, Chiu-Lam A, et al. Magnetic particle imaging-guided heating in vivo using gradient fields for arbitrary localization of magnetic hyperthermia therapy. *ACS Nano*. 2018;12(4):3699–3713. doi:10.1021/acsnano.8b00893

23. Yang X, Shao G, Zhang Y, et al. Applications of magnetic particle imaging in biomedicine. *Front Physiol*. 2022;1(13):898426. doi:10.3389/fphys.2022.898426

24. Arsalani S, Löwa N, Kosch O, et al. Magnetic separation of iron oxide nanoparticles to improve their application for magnetic particle imaging. *Phys Med Biol*. 2021;66(1):015002. doi:10.1088/1361-6560/abcd19

25. Song G, Chen M, Zhang Y, et al. Janus iron oxides @ semiconducting polymer nanoparticle tracer for cell tracking by magnetic particle imaging. *Nano Lett*. 2018;18(1):182–189. doi:10.1021/acs.nanolett.7b03829

26. Arami H, Teeman E, Troksa A, et al. Tomographic magnetic particle imaging of cancer targeted nanoparticles. *Nanoscale*. 2017;9(47):18723–18730. doi:10.1039/C7NR05502A

27. Khandhar AP, Ferguson RM, Arami H, et al. Tuning surface coatings of optimized magnetite nanoparticle tracers for in vivo Magnetic Particle Imaging. *IEEE Trans Magn*. 2015;51(2):5300304. doi:10.1109/TMAG.2014.2321096

28. Chen J, Chen L, Du S, et al. High sensitive detection of circulating tumor cell by multimarker lipid magnetic nanoparticles and clinical verifications. *J Nanobiotechnology*. 2019;17(1):116. doi:10.1186/s12951-019-0548-1

29. Chinnappan R, Faraj AA, Rahman AMA, et al. Anti-VCAM-1 and anti-IL4Rα aptamer-conjugated super paramagnetic iron oxide nanoparticles for enhanced breast cancer diagnosis and therapy. *Molecules*. 2020;25(15):3437. doi:10.3390/molecules25153437

30. Han C, Zhang A, Kong Y, et al. Multifunctional iron oxide-carbon hybrid nanoparticles for targeted fluorescent/MR dual-modal imaging and detection of breast cancer cells. *Anal Chim Acta*. 2019;1(1067):115–128. doi:10.1016/j.aca.2019.03.054

31. Grosenick D, Bremer. C. Fluorescence imaging of breast tumors and gastrointestinal cancer. *Recent Results Cancer Res*. 2020;1(216):591–624.

32. Shen C, Wang X, Zheng Z, et al. Doxorubicin and indocyanine green loaded superparamagnetic iron oxide nanoparticles with PEGylated phospholipid coating for magnetic resonance with fluorescence imaging and chemotherapy of glioma. *Int J Nanomedicine*. 2018;1(14):101–117. doi:10.2147/IJN.S173954

33. Denora N, Lee C, Iacobazzi RM, et al. TSPO-targeted NIR-fluorescent ultra-small iron oxide nanoparticles for glioblastoma imaging. *Eur J Pharm Sci*. 2019;1(139):105047. doi:10.1016/j.ejps.2019.105047

34. Lin R, Huang J, Wang L, et al. Bevacizumab and near infrared probe conjugated iron oxide nanoparticles for vascular endothelial growth factor targeted MR and optical imaging. *Biometer Sci*. 2018;6(6):1517–1525. doi:10.1039/C8BM00225H

35. Dhas N, Kudarha R, Pandey A, et al. Stimuli responsive and receptor targeted iron oxide based nanoplatforms for multimodal therapy and imaging of cancer: conjugation chemistry and alternative therapeutic strategies. *J Control Release*. 2021;333:188–245. doi:10.1016/j.jconrel.2021.03.021

36. Evangelista L, Zattoni F, Cassarino G, et al. PET/MRI in prostate cancer: a systematic review and meta-analysis. *Eur J Nucl Med Mol Imaging*. 2020;48(3):859–873. doi:10.1007/s00259-020-05025-0

37. Alphandéry E. Iron oxide nanoparticles as multimodal imaging tools. *RSC Adv*. 2019;9(69):40577–40587. doi:10.1039/C9RA08612A

38. Namkung S, Zech CJ, Helmberger T, et al. Superparamagnetic iron oxide (SPIO)-enhanced liver MRI with ferucarbotran: efficacy for characterization of focal liver lesions. *J Magn Reson Imaging*. 2007;25(4):755–765. doi:10.1002/jmri.20873

39. Tanaka M, Nakashima O, Wada Y, et al. Pathomorphological study of Kupffer cells in hepatocellular carcinoma and hyperplastic nodular lesions in the liver. *Hepatology*. 1996;24(4):807–812. doi:10.1002/hep.510240409

40. Okada M, Katsube T, Kumano S, et al. Unenhanced fat fraction ratios obtained by MR and enhanced T2* values with liver-specific MR contrast agents for diagnosis of non-alcoholic steatohepatitis in rats. *Acta Radiol*. 2011;52(6):658–664. doi:10.1258/ar.2011.100360

41. Hama Y, Tate. E. Superparamagnetic iron oxide-enhanced MRI-guided stereotactic ablative radiation therapy for liver metastasis. *Rep Pract Oncol Radiother*. 2021;26(3):470–474. doi:10.5603/RPOR.a2021.0052

42. Hama Y, Tate. E. SPIO-enhanced 0.35T MRI-guided radiotherapy for liver malignancies: usefulness in tumor visualization. *Br J Radiol*. 2022;95(1135):20211131. doi:10.1259/bjr.20211131

43. Yue R, Zhang C, Xu L, et al. Dual key co-activated nanoplatform for switchable MRI monitoring accurate ferroptosis-based synergistic therapy. *Chemistry*. 2022;8(7):1956–1981. doi:10.1016/j.chempr.2022.03.009

44. Chen C, Ge J, Gao Y, et al. Ultrasmall superparamagnetic iron oxide nanoparticles: a next generation contrast agent for magnetic resonance imaging. *Wiley Interdiscip Rev Nanomed Nanobiotechnol*. 2022;14(1):e1740. doi:10.1002/wnan.1740

45. Wang L, Huang J, Chen H, et al. Exerting enhanced permeability and retention effect driven delivery by ultrafine iron oxide nanoparticles with T1–T2 switchable magnetic resonance imaging contrast. *ACS Nano*. 2017;11(5):4582–4592. doi:10.1021/acsnano.7b00038

46. Zhang P, Zeng J, Li Y, et al. Quantitative mapping of glutathione within intracranial tumors through interlocked MRI signals of a responsive nanoprobe. *Angew Chem Int Ed*. 2021;60(15):8130–8138. doi:10.1002/anie.202014348

47. Frantellizzi V, Conte M, Pontico M, et al. New frontiers in molecular imaging with Superparamagnetic Iron Oxide Nanoparticles (SPIONs): efficacy, toxicity, and future applications. *Nucl Med Mol Imaging*. 2020;54(2):65–80. doi:10.1007/s13139-020-00635-w

48. Veronesi U, Viale G, Paganelli G, et al. Sentinel lymph node biopsy in breast cancer: ten-year results of a randomized controlled study. *Ann Surg*. 2010;251(4):595–600. doi:10.1097/SLA.0b013e3181c0e92a

49. Krag DN, Anderson SJ, Julian TB, et al. Sentinel-lymph-node resection compared with conventional axillary-lymph-node dissection in clinically node-negative patients with breast cancer: overall survival findings from the NSABP B-32 randomised Phase 3 trial. *Lancet Oncol*. 2010;11(10):927–933. doi:10.1016/S1470-2045(10)70207-2

50. Man V, Wong TT, Co M, et al. Sentinel lymph node biopsy in early breast cancer: magnetic tracer as the only localizing agent. *World J Surg*. 2019;43(8):1991–1996. doi:10.1007/s00268-019-04977-1

51. Aribal E, Çelik L, Yilmaz C, et al. Effects of iron oxide particles on MRI and mammography in breast cancer patients after a sentinel lymph node biopsy with paramagnetic tracers. *Clin Imaging*. 2021;1(75):22–26. doi:10.1016/j.clinimag.2020.12.011

52. Winter A, Chavan A, Wawroschek F. Magnetic resonance imaging of sentinel lymph nodes using intraprostatic injection of superparamagnetic iron oxide nanoparticles in prostate cancer patients: first-in-human results. *Eur Urol*. 2018;73(5):813–814. doi:10.1016/j.eururo.2018.01.009

53. Hamzah JL, Tan BKT, Tan V, et al. A pilot study comparing Sentimag/Sienna versus standard modality for sentinel lymph node identification in patients with breast cancer. *Breast J*. 2020;26(5):1074–1077. doi:10.1111/tbj.13660

54. Sugiyama S, Iwai T, Baba J, et al. MR lymphography with superparamagnetic iron oxide for sentinel lymph node mapping of N0 early oral cancer: a pilot study. *Dentomaxillofac Radiol*. 2020;50(4):20200333. doi:10.1259/dmfr.20200333

55. Murakami K, Kotani Y, Suzuki A, et al. Superparamagnetic iron oxide as a tracer for sentinel lymph node detection in uterine cancer: a pilot study. *Sci Rep*. 2020;10(1):7945. doi:10.1038/s41598-020-64926-0

56. Alvarado MD, Mittendorf EA, Teshome M, et al. SentimagIC: a non-inferiority trial comparing superparamagnetic iron oxide versus technetium-99m and blue dye in the detection of axillary sentinel nodes in patients with early-stage breast cancer. *Ann Surg Oncol*. 2019;26 (11):3510–3516. doi:10.1245/s10434-019-07577-4

57. Taruno K, Kurita T, Kuwahata A, et al. Multicenter clinical trial on sentinel lymph node biopsy using superparamagnetic iron oxide nanoparticles and a novel handheld magnetic probe. *J Surg Oncol*. 2019;120(8):1391–1396. doi:10.1002/jso.25747

58. Pouw JJ, Grootendorst MR, Bezooijen R, et al. Pre-operative sentinel lymph node localization in breast cancer with superparamagnetic iron oxide MRI: the SentiMAG multicentre trial imaging subprotocol. *Br J Radiol*. 2015;88(1056):20150634. doi:10.1259/bjr.20150634

59. Liang X, Yu J, Wen B, et al. MRI and FDG-PET/CT based assessment of axillary lymph node metastasis in early breast cancer: a meta-analysis. *Clin Radiol*. 2017;72(4):295–301. doi:10.1016/j.crad.2016.12.001

60. Winter A, Kowald T, Engels S, et al. Magnetic resonance sentinel lymph node imaging and magnetometer-guided intraoperative detection in penile cancer, using superparamagnetic iron oxide nanoparticles: first results. *Urol Int*. 2020;104(3–4):177–180. doi:10.1159/000502017

61. Johnson L, Pinder SE, Douek. M. Deposition of superparamagnetic iron-oxide nanoparticles in axillary sentinel lymph nodes following subcutaneous injection. *Histopathology*. 2013;62(3):481–486. doi:10.1111/his.12019

62. Winter A, Engels S, Goos P, et al. Accuracy of magnetometer-guided sentinel lymphadenectomy after intraprostatic injection of super-paramagnetic iron oxide nanoparticles in prostate cancer: the sentimag pro II study. *Cancers*. 2019;12(1):32. doi:10.3390/cancers12010032

63. Winter A, Kowald T, Paulo TS, et al. Magnetic resonance sentinel lymph node imaging and magnetometer-guided intraoperative detection in prostate cancer using superparamagnetic iron oxide nanoparticles. *Int J Nanomedicine*. 2018;1(13):6689–6698. doi:10.2147/IJN.S173182

64. Savolainen H, Volpe A, Phinikaridou A, et al. 68Ga-Sienna+ for PET-MRI guided sentinel lymph node biopsy: synthesis and preclinical evaluation in a metastatic breast cancer model. *Nanotheranostics*. 2019;3(3):255–265. doi:10.7150/ntno.34727

65. Stadnik TW, Everaert H, Makkat S, et al. Breast imaging. Preoperative breast cancer staging: comparison of USPIO-enhanced MR imaging and 18F-fluorodeoxyglucose (FDC) positron emission tomography (PET) imaging for axillary lymph node staging—initial findings. *Eur Radiol*. 2006;16(10):2153–2160. doi:10.1007/s00330-006-0276-4

66. Shams S, Lippold K, Blohmer JU, et al. A pilot study evaluating the effects of magtrace® for sentinel node biopsy in breast cancer patients regarding care process optimization, reimbursement, surgical time, and patient comfort compared with standard technetium99. *Ann Surg Oncol*. 2021;28(6):3232–3240. doi:10.1245/s10434-020-09280-1

67. Karakatsanis A, Daskalakis K, Stålberg P, et al. Superparamagnetic iron oxide nanoparticles as the sole method for sentinel node biopsy detection in patients with breast cancer. *Br J Surg*. 2017;104(12):1675–1685. doi:10.1002/bjs.10606

68. Wiebke Geißen SE, Aust P, Schiffmann J, Gerullis H, Wawroschek F, Winter A. Diagnostic accuracy of magnetometer-guided sentinel lymphadenectomy after intraprostatic injection of superparamagnetic iron oxide nanoparticles in intermediate- and high-risk prostate cancer using the magnetic activity of sentinel nodes. *Front Pharmacol*. 2019;1(10):1123. doi:10.3389/fphar.2019.01123

69. Lu C, Han L, Wang J, et al. Engineering of magnetic nanoparticles as magnetic particle imaging tracers. *Chem Soc Rev*. 2021;50 (14):8102–8146. doi:10.1039/d0cs00260g

70. Tay PCZW, Hensley D, Zhou XY, et al. Using magnetic particle imaging systems to localize and guide magnetic hyperthermia treatment: tracers, hardware, and future medical applications. *Theranostics*. 2020;10(7):2965–2981. doi:10.7150/thno.40858

71. Du Y, Liu X, Liang Q, et al. Optimization and design of magnetic ferrite nanoparticles with uniform tumor distribution for highly sensitive MRI/MPI performance and improved magnetic hyperthermia therapy. *Nano Lett*. 2019;19(6):3618–3626. doi:10.1021/acs.nanolett.9b00630

72. Hensley D, Tay ZW, Dhavalikar R, et al. Combining magnetic particle imaging and magnetic fluid hyperthermia in a theranostic platform. *Phys Med Biol*. 2017;62(9):3483–3500. doi:10.1088/1361-6560/aa5601

73. Koda M, Tokunaga S, Miyoshi K, et al. Ablative margin states by magnetic resonance imaging with ferucarbotran in radiofrequency ablation for hepatocellular carcinoma can predict local tumor progression. *J Gastroenterol*. 2013;48(11):1283–1292. doi:10.1007/s00535-012-0747-0

74. Nagai M, Yamaguchi M, Mori K, et al. Magnetic resonance-based visualization of thermal ablative margins around hepatic tumors by means of systemic ferucarbotran administration before radiofrequency ablation. *Invest Radiol*. 2015;50(6):376–383. doi:10.1097/RLI.0000000000000137

75. Mori K, Fukuda K, Asaoka H, et al. Radiofrequency ablation of the liver: determination of ablative margin at MR imaging with impaired clearance of ferucarbotran--feasibility study. *Radiology*. 2009;251(2):557–565. doi:10.1148/radiol.2512081161

76. Furuta T, Yamaguchi M, Nakagami R, et al. Delayed hepatic signal recovery on ferucarbotran-enhanced magnetic resonance images in a rat model with regional liver irradiation. *Magn Reson Mater Phys Biol Med*. 2014;27(6):501–508. doi:10.1007/s10334-014-0434-7

77. Kakite S, Fujii S, Nakamatsu S, et al. Usefulness of administration of SPIO prior to RF ablation for evaluation of the therapeutic effect: an experimental study using miniature pigs. *Eur J Radiol*. 2011;78(2):282–286. doi:10.1016/j.ejrad.2011.01.048

78. Furuta T, Yamaguchi M, Minami M, et al. Persistent T2*-hypointensity of the liver parenchyma after irradiation to the SPIO-accumulated liver: an imaging marker for responses to radiotherapy in hepatic malignancies. *J Magn Reson Imaging*. 2017;45(1):303–312. doi:10.1002/jmri.25350

79. Furuta T, Yamaguchi M, Minami M, et al. Treatment margins in radiotherapy for liver tumors visualized as T2*-hypointense areas on SPIO-enhanced MRI at 9.4 T. *MAGMA*. 2020;33(5):701–712. doi:10.1007/s10334-020-00838-4

80. Fukuda K, Mori K, Hasegawa N, et al. Safety margin of radiofrequency ablation for hepatocellular carcinoma: a prospective study using magnetic resonance imaging with superparamagnetic iron oxide. *Jpn J Radiol*. 2019;37(7):555–563. doi:10.1007/s11604-019-00843-1

81. Zuazo-Gaztelu I, Casanovas. O. Unraveling the role of angiogenesis in cancer ecosystems. *Front Oncol*. 2018;1(8):248. doi:10.3389/fonc.2018.00248

82. Pike MM, Stoops CN, Langford CP, et al. High-resolution longitudinal assessment of flow and permeability in mouse glioma vasculature: sequential small molecule and SPIO dynamic contrast agent MRI. *Magn Reson Med*. 2009;61(3):615–625. doi:10.1002/mrm.21931

83. Robinson SP, Boult JKR, Vasudev NS, et al. Monitoring the vascular response and resistance to sunitinib in renal cell carcinoma in vivo with susceptibility contrast MRI. *Cancer Res*. 2017;77(15):4127–4134. doi:10.1158/0008-5472.CAN-17-0248

84. Kim J, Kim E, Euceda LR, et al. Multiparametric characterization of response to anti-angiogenic therapy using USPIO contrast-enhanced MRI in combination with dynamic contrast-enhanced MRI. *J Magn Reson Imaging*. 2018;47(6):1589–1600. doi:10.1002/jmri.25898

85. Yang S-H, Lin J, Lu F, et al. Contrast-enhanced susceptibility weighted imaging with ultrasmall superparamagnetic iron oxide improves the detection of tumor vascularity in a hepatocellular carcinoma nude mouse model. *J Magn Reson Imaging*. 2016;44(2):288–295. doi:10.1002/jmri.25167

86. Muldoon LL, Gahramanov S, Li X, et al. Dynamic magnetic resonance imaging assessment of vascular targeting agent effects in rat intracerebral tumor models. *Neuro Oncol*. 2010;13(1):51–60. doi:10.1093/neuonc/noq150

87. Yang S, Lin J, Lu F, et al. Use of ultrasmall superparamagnetic iron oxide enhanced susceptibility weighted imaging and mean vessel density imaging to monitor antiangiogenic effects of sorafenib on experimental hepatocellular carcinoma. *Contrast Media Mol Imaging*. 2017;1 (2017):9265098.

88. Farrell BT, Hamilton BE, Dósa E, et al. Using iron oxide nanoparticles to diagnose CNS inflammatory diseases and PCNSL. *Neurology*. 2013;81(3):256–263. doi:10.1212/WNL.0b013e31829bfd8f

89. Gahramanov S, Raslan AM, Muldoon LL, et al. Potential for differentiation of pseudoprogression from true tumor progression with dynamic susceptibility-weighted contrast-enhanced magnetic resonance imaging using ferumoxytol vs gadoteridol: a pilot study. *Int J Radiat Oncol Biol Phys*. 2011;79(2):514–523.

90. Varallyay CG, Nesbit E, Fu R, et al. High-resolution steady-state cerebral blood volume maps in patients with central nervous system neoplasms using ferumoxytol, a superparamagnetic iron oxide nanoparticle. *J Cereb Blood Flow Metab*. 2013;33(5):780–786. doi:10.1038/jcbfm.2013.36

91. Saito K, Ledsam J, Sourbron S, et al. Validation study of perfusion parameter in hypervascular hepatocellular carcinoma and focal nodular hyperplasia using dynamic susceptibility magnetic resonance imaging with super-paramagnetic iron oxide: comparison with single level dynamic CT arteriography. *Quant Imaging Med Surg*. 2020;10(6):1298–1306. doi:10.21037/qims-18-233

92. Chakhoyan A, Yao J, Leu K, et al. Validation of vessel size imaging (VSI) in high-grade human gliomas using magnetic resonance imaging, image-guided biopsies, and quantitative immunohistochemistry. *Sci Rep*. 2019;9(1):2846. doi:10.1038/s41598-018-37564-w

93. Pak S, Suh YS, Lee D-E, et al. Association between postoperative detection of circulating tumor cells and recurrence in patients with prostate cancer. *J Urol*. 2020;203(6):1128–1134. doi:10.1097/JU.0000000000000704

94. Tan Y, Wu. H. The significant prognostic value of circulating tumor cells in colorectal cancer: a systematic review and meta-analysis. *Curr Probl Cancer*. 2018;42(1):95–106. doi:10.1016/j.currproblcancer.2017.11.002

95. Banys-Paluchowski M, Fehm T, Janni W, et al. Circulating and disseminated tumor cells in breast carcinoma: report from the consensus conference on tumor cell dissemination during the 39th annual meeting of the German Society of Senology, Berlin, 27 June 2019. *Geburtshilfe Frauenheilkd*. 2019;79(12):1320–1327. doi:10.1055/a-1031-1120

96. Lin M, Liang S-Z, Shi J, et al. Circulating tumor cell as a biomarker for evaluating allogenic NK cell immunotherapy on stage IV non-small cell lung cancer. *Immunol Lett*. 2017;1(191):10–15. doi:10.1016/j.imlet.2017.09.004

97. Gee MS, Ghazani AA, Haq R, et al. Point of care assessment of melanoma tumor signaling and metastatic burden from μNMR analysis of tumor fine needle aspirates and peripheral blood. *Nanomed Nanotechnol Biol Med*. 2017;13(3):821–828. doi:10.1016/j.nano.2016.12.006

98. Ghazani AA, Castro CM, Gorbatov R, et al. Sensitive and direct detection of circulating tumor cells by multimarker μ-nuclear magnetic resonance. *Neoplasia*. 2012;14(5):388–395. doi:10.1596/neo.12696

99. Ghazani AA, McDermott S, Pectasides M, et al. Comparison of select cancer biomarkers in human circulating and bulk tumor cells using magnetic nanoparticles and a miniaturized micro-NMR system. *Nanomed Nanotechnol Biol Med*. 2013;9(7):1009–1017. doi:10.1016/j.nano.2013.03.011

100. Suresh D, Ghoshdastidar S, Gangula A, et al. Magnetic iron nanocubes effectively capture epithelial and mesenchymal cancer cells. *ACS Omega*. 2020;5(37):23724–23735. doi:10.1021/acsomega.0c02699

101. Xu H, Aguilar ZP, Yang L, et al. Antibody conjugated magnetic iron oxide nanoparticles for cancer cell separation in fresh whole blood. *Biomaterials*. 2011;32(36):9758–9765. doi:10.1016/j.biomaterials.2011.08.076

102. Wu -L-L, Wen C-Y, Hu J, et al. Nanosphere-based one-step strategy for efficient and nondestructive detection of circulating tumor cells. *Biosens Bioelectron*. 2017;1(94):219–226. doi:10.1016/j.bios.2017.03.009

103. Miller MC, Doyle GV, Terstappen. LWMM. Significance of circulating tumor cells detected by the cellsearch system in patients with metastatic breast colorectal and prostate cancer. *J Oncol*. 2010;1(2010):1–8. doi:10.1155/2010/617421

104. Castro CM, Ghazani AA, Chung J, et al. Miniaturized nuclear magnetic resonance platform for detection and profiling of circulating tumor cells. *Lab Chip*. 2014;14(1):14–23. doi:10.1039/C3LC50621E

105. Chiang C-S, Kao Y-C, Webster TJ, et al. Circulating tumor-cell-targeting Au-nanocage-mediated bimodal phototherapeutic properties enriched by magnetic nanocores. *J Mater Chem B*. 2020;8(25):5460–5471. doi:10.1039/D0TB00501K

106. Wu -L-L, Zhang Z-L, Tang M, et al. Spectrally combined encoding for profiling heterogeneous circulating tumor cells using a multifunctional nanosphere-mediated microfluidic platform. *Angew Chem Int Ed*. 2020;59(28):11240–11244. doi:10.1002/anie.201914468

107. Glover JC, Aswendt M, Boulland J-L, et al. In vivo cell tracking using non-invasive imaging of iron oxide-based particles with particular relevance for stem cell-based treatments of neurological and cardiac disease. *Mol Imaging Biol*. 2020;22(6):1469–1488. doi:10.1007/s11307-019-01440-4

108. Galli F, Varani M, Lauri C, et al. Immune cell labelling and tracking: implications for adoptive cell transfer therapies. *EJNMMI Radiopharm Chem*. 2021;6(1):7. doi:10.1186/s41181-020-00116-7

109. Thin MZ, Allan H, Bofinger R, et al. Multi-modal imaging probe for assessing the efficiency of stem cell delivery to orthotopic breast tumours. *Nanoscale*. 2020;12(31):16570–16585. doi:10.1039/D0NR03237A

110. Rajendran RL, Jogalekar MP, Gangadaran P, et al. Noninvasive in vivo cell tracking using molecular imaging: a useful tool for developing mesenchymal stem cell-based cancer treatment. *World J Stem Cells*. 2020;12(12):1492–1510. doi:10.4252/wjsc.v12.i12.1492

111. Jasmin, Souza GTD, Louzada RA, et al. Tracking stem cells with superparamagnetic iron oxide nanoparticles: perspectives and considerations. *Int J Nanomedicine*. 2017;1(12):779–793. doi:10.2147/IJN.S126530

112. Li L, Jiang W, Luo K, et al. Superparamagnetic iron oxide nanoparticles as MRI contrast agents for non-invasive stem cell labeling and tracking. *Theranostics*. 2013;3(8):595–615. doi:10.7150/thno.5366

113. Liu H, Lu C, Han L, et al. Optical – magnetic probe for evaluating cancer therapy. *Coord Chem Rev*. 2021;441:213978. doi:10.1016/j.ccr.2021.213978

114. Xie T, Chen X, Fang J, et al. Non-invasive monitoring of the kinetic infiltration and therapeutic efficacy of nanoparticle-labeled chimeric antigen receptor T cells in glioblastoma via 7.0-Tesla magnetic resonance imaging. *Cytotherapy*. 2021;23(3):211–222. doi:10.1016/j.jcyt.2020.10.006

115. Bengtsson NE, Kim S, Lin L, et al. Ultra-high-field MRI real-time imaging of HSC engraftment of the bone marrow niche. *Leukemia*. 2011;25 (8):1223–1231. doi:10.1038/leu.2011.72

116. Walczak P, Kedziorek DA, Gilad AA, et al. Applicability and limitations of MR tracking of neural stem cells with asymmetric cell division and rapid turnover: the case of the shiverer dysmyelinated mouse brain. *Magn Reson Med*. 2007;58(2):261–269. doi:10.1002/mrm.21280

117. Couvreur P. Nanomedicine: from where are we coming and where are we going? *J Control Release*. 2019;1(311–312):319–321.

118. Golombek SK, May J-N, Theek B, et al. Tumor targeting via EPR: strategies to enhance patient responses. *Adv Drug Del Rev*. 2018;1 (130):17–38. doi:10.1016/j.addr.2018.07.007

119. Chen L, Zang F, Wu H, et al. Using PEGylated magnetic nanoparticles to describe the EPR effect in tumor for predicting therapeutic efficacy of micelle drugs. *Nanoscale*. 2018;10(4):1788–1797. doi:10.1039/C7NR08319J

120. Miller MA, Gadde S, Pfirschke C, et al. Predicting therapeutic nanomedicine efficacy using a companion magnetic resonance imaging nanoparticle. *Sci Transl Med*. 2015;7(314):314ra183. doi:10.1126/scitranslmed.aac6522

121. Ramanathan RK, Korn RL, Raghunand N, et al. Correlation between ferumoxytol uptake in tumor lesions by MRI and response to nanoliposomal irinotecan in patients with advanced solid tumors: a pilot study. *Clin Cancer Res*. 2017;23(14):3638–3648. doi:10.1158/1078-0432.CCR-16-1990

122. Schleich N, Sibret P, Danhier P, et al. Dual anticancer drug/superparamagnetic iron oxide-loaded PLGA-based nanoparticles for cancer therapy and magnetic resonance imaging. *Int J Pharm*. 2013;447(1–2):94–101. doi:10.1016/j.ijpharm.2013.02.042

123. Luque-Michel E, Sebastian V, Larrea A, et al. Co-encapsulation of superparamagnetic nanoparticles and doxorubicin in PLGA nanocarriers: development, characterization and in vitro antitumor efficacy in glioma cells. *Eur J Pharm Biopharm*. 2019;1(145):65–75. doi:10.1016/j.ejpb.2019.10.004

124. Zheng X-C, Ren W, Zhang S, et al. The theranostic efficiency of tumor-specific, pH-responsive, peptide-modified, liposome-containing paclitaxel and superparamagnetic iron oxide nanoparticles. *Int J Nanomedicine*. 2018;1(13):1495–1504. doi:10.2147/IJN.S157082

125. Pan C, Liu Y, Zhou M, et al. Theranostic pH-sensitive nanoparticles for highly efficient targeted delivery of doxorubicin for breast tumor treatment. *Int J Nanomedicine*. 2018;13:1119–1137. doi:10.2147/IJN.S147464

126. Miller MA, Arlauckas S, Weissleder. R. Prediction of anti-cancer nanotherapy efficacy by imaging. *Nanotheranostics*. 2017;1(3):296–312. doi:10.7150/ntno.20564

127. Karimian-Jazi K, Münch P, Alexander A, et al. Monitoring innate immune cell dynamics in the glioma microenvironment by magnetic resonance imaging and multiphoton microscopy (MR-MPM). *Theranostics*. 2020;10(4):1873–1883. doi:10.7150/thno.38659